iScience

CellPress

Article

Blueberry Extract Improves Obesity through Regulation of the Gut Microbiota and Bile Acids via Pathways Involving FXR and TGR5

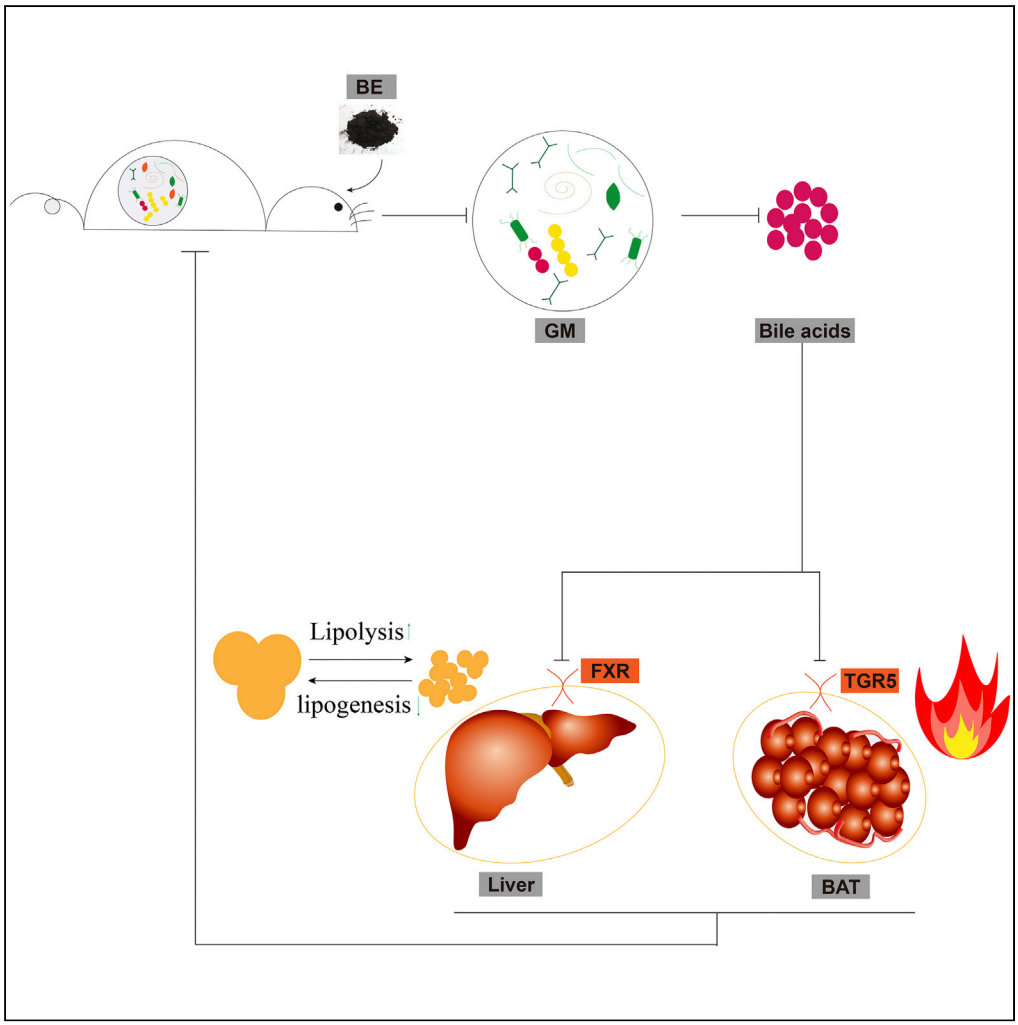

Jielong Guo, Xue Han, Hongyu Tan, Weidong Huang, Yilin You, Jicheng Zhan

huanggwd@263.net (W.H.)
yilinyou@cau.edu.cn (Y.Y.)
zhanjicheng@cau.edu.cn (J.Z.)

HIGHLIGHTS

Blueberry extract (BE) treatment improved obesity-related metabolic syndromes in mice

BE treatment regulated the plasma bile acid (BA) pool through gut microbiota

BE treatment decreased serum-conjugated BA contents and increased free secondary BAs

BE treatment activated BA receptors TGR5 and FXR in brown adipose tissue and liver

Guo et al., iScience 19, 676–690
September 27, 2019
https://doi.org/10.1016/j.isci.2019.08.020

iScience

CellPress

Article

Blueberry Extract Improves Obesity through Regulation of the Gut Microbiota and Bile Acids via Pathways Involving FXR and TGR5

Jielong Guo,[1,2] Xue Han,[1] Hongyu Tan,[1] Weidong Huang,[1,*] Yilin You,[1,2,*] and Jicheng Zhan[1,3,*]

SUMMARY

The metabolic improvement effect of blueberries has long been recognized, although its precise mechanism(s) remains obscure. Here, we show that phenolic blueberry extract (BE) treatment improved diet- and genetically induced metabolic syndromes, which were linked to increased energy expenditure in brown adipose tissue (BAT) and improved lipid metabolism in the liver via pathways involving the bile acid (BA) receptors TGR5 and FXR. These observations were strongly correlated with the regulation of BAs (e.g., a decrease in the FXR inhibitors TαMCA and TβMCA) and the gut microbiota (GM) (e.g., an expansion of *Bifidobacteria* and *Lactobacillus*), because antibiotic treatment completely blunted the regulation of the GM and BAs and the metabolic effects of BE. We also observed similar results in *db/db* mice. Furthermore, treating mouse primary cells derived from the liver and BAT with the combinations of BAs mimicking the *in vivo* alterations upon BE treatment mirrored the *in vivo* observations in mice.

INTRODUCTION

The antimetabolic disease function of plant polyphenols (PPs) has long been noted by researchers studying the "health secrets" of people following Mediterranean diet, which contains abundant PPs (Kastorini et al., 2011). Numerous animal and human studies have demonstrated that, although controversial, PPs from fruits, vegetables, and wines can improve diet-induced obesity and its related metabolic syndromes, including inflammation and insulin resistance (IR) (Han et al., 2018; Tresserra-Rimbau et al., 2015). Certain mechanisms underlying these phenotypes have been studied, such as the inhibition of α-glucosidase, enhancement of pancreatic β-cell function, and regulation of liver function (Hanhineva et al., 2010). However, the reasons for these effects are unclear, as most natural PPs cannot be absorbed directly by mammals, and the plasma concentration of natural PPs or their metabolites is low, making it difficult to fulfill their physiological function (Kay et al., 2017).

Recently, the regulation of the gut microbiota (GM) by PPs has received more attention for its potential to improve metabolism. The GM of mammals has fundamental impacts on the host's health in many aspects, such as immunity, psychology, behavior and, especially, energy metabolism (Turnbaugh et al., 2006; Bäckhed et al., 2004). The GM plays a significant role in regulating the body weight (BW) of hosts (Ridaura et al., 2013). Metabolites of the GM are important in regulating the host's metabolism, and, among others, bile acids (BAs) play a key role (Swann et al., 2011). BAs are synthesized from cholesterol and conjugated to taurine (mouse) or glycine (human) in the liver before being released into the intestine, where they meet microbes. The GM can convert conjugated primary BAs to free BAs via bile salt hydrolase (BSH) and then further to secondary BAs through dehydroxylation and dehydrogenation (Just et al., 2018). BAs can modulate energy homeostasis through G protein-coupled bile acid receptor 1 (GPBAR1, also known as TGR5) and farnesoid X receptor (FXR, also known as BAR). Supplementation with cholic acid (CA) prevented diet-induced obesity and its related metabolic syndromes in mice via the activation of TGR5 (Watanabe et al., 2006).

Blueberries (*Vaccinium spp.*) are rich in PPs (mainly anthocyanins) and known for their antioxidant and cardiovascular protective function (Neto, 2010). It has been shown that blueberries (or their phenolic extract) were able to ameliorate high-fat diet (HFD)-induced obesity and related metabolic syndromes such as hyperglycemia and IR and to regulate the GM composition (Stull et al., 2010; Defuria et al., 2009). However, although a correlation between the regulation of the GM and an improvement in metabolism has been observed, neither has the causal link of this relationship nor has the mechanism of this

[1]College of Food Science and Nutritional Engineering, Beijing Key Laboratory of Viticulture and Enology, China Agricultural University, Beijing 100083, China

[2]Xinghua Industrial Research Centre for Food Science and Human Health, China Agricultural University, Xinghua 225700, Jiangsu, China

[3]Lead Contact

*Correspondence: huanggwd@263.net (W.H.), yilinyou@cau.edu.cn (Y.Y.), zhanjicheng@cau.edu.cn (J.Z.)

https://doi.org/10.1016/j.isci.2019.08.020

connection been studied yet (Lee et al., 2018). To investigate the correlation between blueberry PPs, the GM, and metabolism, we performed four independent experiments (three mouse studies and one *in vitro* study, more details seen in Transparent Methods-Animals and Cell Separation and Culture) employing both mouse and mouse primary cells. The results of this study have implications for understanding the mechanism(s) of the effects of dietary PPs on health and the relationship between the GM and host metabolism.

RESULTS

Blueberry Extract Alleviates Obesity and Liver Steatosis in Diet-Induced Obese Mice

We obtained 2.81 ± 0.23 g extract, including 79.62% phenolic compounds, from 100 g fresh blueberry fruit. The hexosides of delphinidin, malvidin, petunidin, cyanidin, myricetin, and quercetin as well as 5-caffeoylquinic acid, vanillic acid, and proanthocyanidins were identified as the most abundant components of the blueberry extract (BE) (Table S1).

For mouse study 1- and 3-week old C57BL/6 male mice were randomly assigned to four groups after adapting for 1 week as follows: (1) a CHOW1 group fed a standard chow diet (3.85 kcal/g, 10% energy from fat), (2) an HFD1 group fed an HFD (4.73 kcal/g, 60% energy from fat), (3) a CBE group (5 gL^{-1} BE in drinking water) fed a standard chow diet, and (4) a BE1 group (0.5% (m/v) BE in drinking water) fed an HFD. BE treatment significantly reduced diet-induced weight gain from the sixth week of the study until the end of the study, and these findings were not related to energy intake or excretion (Figures 1A, 1B, and 1D). Moreover, the water consumption was also not influenced by BE treatment (Figure 1C). BE-treated mice had reduced body fat, especially in the inguinal white adipose tissue (iWAT), epididymal white adipose tissue (eWAT), and liver (Figures 1E, 1K, 1L, 2F, and 2G). Liver steatosis and damage induced by an HFD were significantly ameliorated through BE administration, as indicated by decreased hepatic and plasma concentrations of triacylglycerol (TG) (Figure 1F) and a reduction in plasma lactate dehydrogenase, alanine transaminase, and aspartate aminotransferase content (Figure 1G). BE-treated mice showed an increased energy expenditure (Figure 1H), which was not related to physical activity (Figure 1I); consistent with this, the core body temperature of BE-treated mice was higher than that of the vehicle-treated HFD-fed mice (Figure 1J). Notably, BE treatment had no significant influence on the metabolism of mice fed a chow diet, as shown by parameters such as BW, tissue weight, fat deposition, and plasma biochemical parameters compared with those of chow-fed control mice (Figure 1). Taken together, these results showed that BE administration reduced HFD-induced weight gain and adiposity (partially) by increasing energy expenditure and thermogenesis.

BE Treatment Ameliorates Increased Intestinal Permeability and Systemic Inflammation Triggered by an HFD and Improves Glucose Metabolism

BE treatment alleviated the increased permeability of the colon and distal ileum triggered by an HFD, as indicated by the increased MUC2 levels in the colon and increased mRNA expression of occludin and tight junction protein 1 (TJP1, also known as ZO-1) both in the ileum and colon compared with their expression in mice in the HFD1 group (Figures 2A and 2B), which was accompanied by a reduction in the mRNA levels of genes related to inflammation, including toll-like receptor 4 (TLR4), interleukin 6 (IL-6), and tumor necrosis factor alpha (TNF-α) (Figure 2C). We also found an improvement in inflammation in white adipose tissue (WAT) and the liver in BE-treated mice, as indicated by the reduced mRNA expression of TLR4, IL-6, and TNF-α and the decreased adipocyte size in the WAT (Figures 2C, 2F and 2G). Consistent with these results, the plasma concentrations of lipopolysaccharides (LPS), IL-6, and TNF-α were also decreased in BE-treated mice compared with those in vehicle-treated HFD-fed mice (Figure 2D).

Glucose metabolism is closely related to systemic inflammation (Gregor and Hotamisligil, 2011). As expected, BE-treated mice showed profoundly improved glucose intolerance and insulin sensitivity (Figure 2D). Notably, leptin, a key modulator of energy homeostasis that is usually irregularly high in obese individuals (Friedman and Halaas, 1998), was lower in the plasma of mice in the BE1 group than in mice in the HFD1 group, and, consistent with this, BE-treated mice showed reduced mRNA expression of CCAAT enhancer-binding proteins β and σ (CEBPβ and CEBPσ) in the iWAT (Figure 2E). Similar to the previous observations, systemic inflammation and glucose metabolism in BE-treated chow-fed mice resembled those of vehicle-treated chow-fed mice. Collectively, these results showed that BE administration enhanced the expression of genes related with intestinal barrier integrity, decreased systemic inflammation, and improved glucose metabolism.

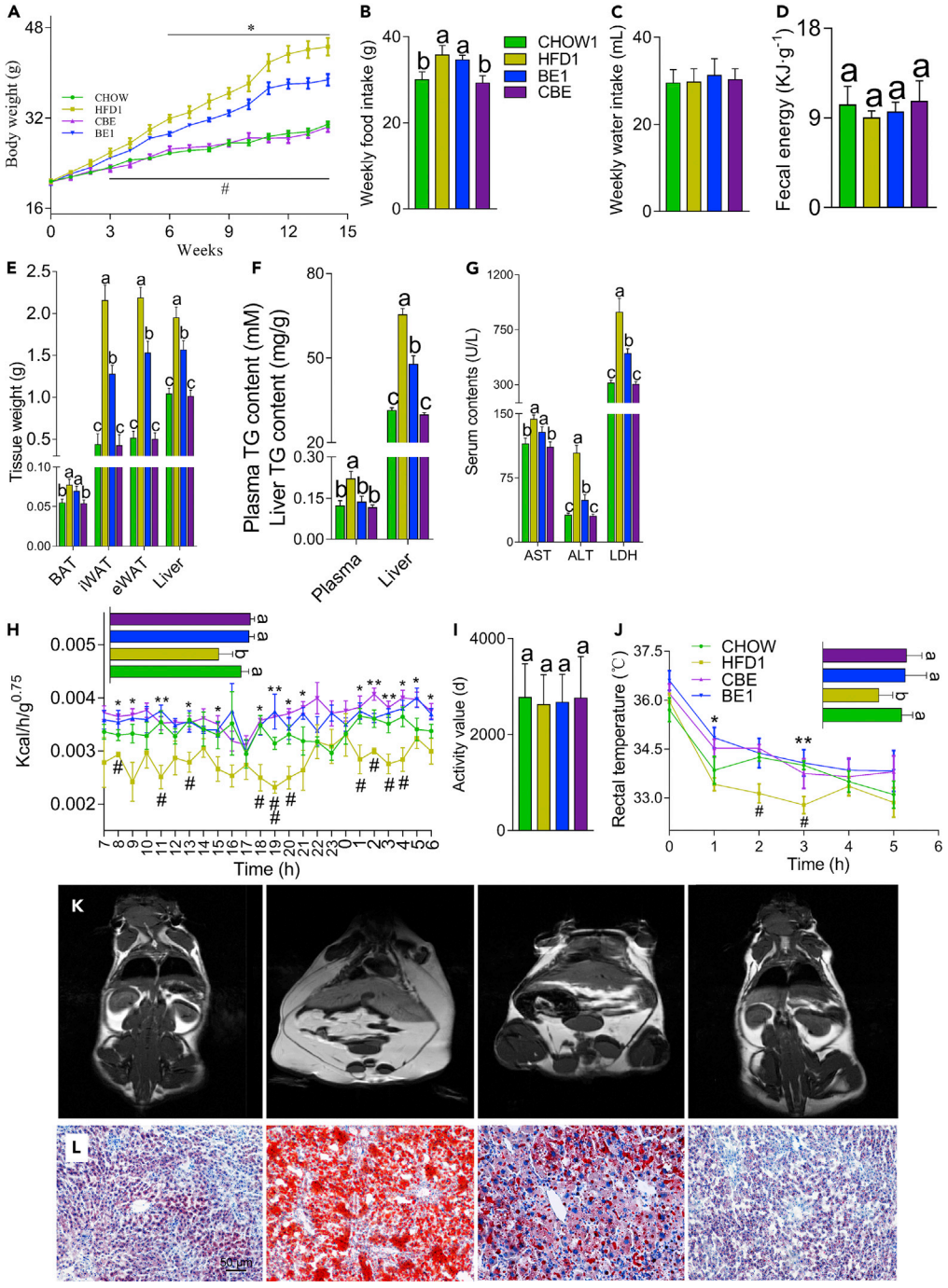

Figure 1. BE Treatment Alleviated Obesity, Reduced Liver Steatosis, and Increased Energy Expenditure

(A) The body weight change of mice throughout the experiment in study 1.

(B–D) The weekly food intake (B), water intake (C), and fecal energy (D) of mice in study 1.

(E) Tissue weights.

(F) The TG concentration in the plasma and liver.

(G) Plasma concentrations of AST, ALT, and LDH, respectively.

(H and I) BE treatment increased the energy expenditure of mice fed an HFD (H), which was not related to physical activity (I).

(J) The alteration in rectal temperature following cold stimulation and the relative area under the curve (AUC).

Figure 1. *Continued*

(K) Magnetic resonance imaging graphs of the CHOW1, HFD1 BE1, and CBE groups (from left to right). The white areas represent lipids, n = 8.

(L) Representative oil red O staining of the livers of mice from the CHOW1, HFD1 BE1, and CBE groups (from left to right), n = 8.

For all figures, *p < 0.05 and **p < 0.01 for BE1 versus HFD1, $^{\#}p < 0.05$ and $^{\#\#}p < 0.01$ for CHOW1 versus HFD1 and different letters indicate a significant difference between columns, p < 0.05.

BE Improves the GM Disturbed by HFD

Based on the above results, we concluded that BE administration had a minimal influence on the metabolism of mice fed a chow diet; therefore, we excluded the mice in the CBE group in the following analysis and experiments. Fourteen weeks of treatment with an HFD decreased the richness of the GM and resulted in an abnormal Bacteroidetes to Fimicutes ratio in the HFD1 mice, which were completely restored through BE administration (Figures 3A and 3E). Intergroup analysis based on the unweighted UniFrac distance showed that BE-treated mice were more similar to mice fed a chow diet (Figure 3D) than vehicle-treated HFD-fed mice. Principal coordinate analysis based on the unweighted UniFrac distance also revealed that BE-treated mice were clustered apart from vehicle-treated HFD-fed mice and partially overlapped with mice fed a chow diet (Figure 3D).

We employed the linear discriminant analysis effect size (LEfSe) approach to determine the bacterial taxa notably influenced by BE treatment. Consistent with the above results, taxa belonging to the phyla Bacteroidetes and Firmicutes, such as Ruminococcaceae and Bacteroidaceae, were the main features discriminating the GM of BE-treated mice from that of vehicle-treated HFD-fed mice (Figure 3C). In addition, the expansion of *Akkermansia* and *Bifidobacterium* along with a significant decrease in the *Desulfovibrio* and *Bilophila* genera was observed in mice in the BE1 group (Figure 3C). Moreover, the abundance of the significant taxa identified through LEfSe analysis was considerably high, as determined through sequencing and qPCR (Figures 3B and 3C). Collectively, these results demonstrated a substantial alteration and improvement in the GM through BE administration.

BE Changes the Plasma Bile Acid Pool, Promotes the Activation of BAT and the Browning of WAT, and Improves Lipid Metabolism in the Liver and Adipose Tissue

As BA metabolism is closely connected with the GM, and they are important regulators of energy homeostasis (Swann et al., 2011), we sought to determine the influence of BE administration on the BA pool and metabolism. BE administration substantially decreased the augmented plasma BA size induced by an HFD, and conjugated BAs, including tauro-α-muricholic acid (TαMCA), TβMCA, and taurocholic acid (TCA), were the most reduced BAs, among others (Figure 3F). Among other highly abundant BAs, lithocholic acid (LCA) and chenodeoxycholic acid (CDCA) were increased; CA, deoxycholic acid (DCA), ursodeoxycholic acid, and tauroursodeoxycholic acid (TUDCA) were not influenced; and hyodeoxycholic acid (HDCA) and tauro-HDCA were decreased in BE-treated mice compared with their levels in mice in the HFD1 group (Figure 3F). Furthermore, the ratios of primary to secondary as well as conjugated to unconjugated BAs were decreased following BE treatment (Figure 3F). The *Bifidobacterium* and *Bacteroides* genera, known to produce BSH (Gerard, 2013), were strongly positively correlated with some unconjugated BAs (e.g., LCA and CA) in the plasma and negatively related to taurine-conjugated BAs including TαMCA, TβMCA, and TCA (Figure S1C). The fecal BA level was slightly (p = 0.27) increased, whereas the mRNA expression of ileal bile acid transporter (IBAT, also known as SLC10A2 and ABST) was not influenced by BE treatment (Figure 3F), suggesting that the increase in secondary BAs may contribute to the reduced intestinal reabsorption of BAs (Sayin et al., 2013). Collectively, these results showed that BE administration altered the plasma BA pool and the GM and that there was a strong correlation between the alteration of BA pool and GM.

FXR, an important nuclear BA receptor, controls the expression of various genes related to lipid metabolism, such as sterol-regulatory element binding proteins-1c (SREBP-1c) and carbohydrate-responsive element-binding protein (ChREBP), in the liver (Molinaro et al., 2018). As BE administration sharply decreased the plasma levels of TαMCA and TβMCA, FXR antagonists (Sayin et al., 2013), we assessed the influence of their reduced levels on FXR-dependent lipid metabolism. As expected, both the mRNA and protein levels of FXRα and small heterodimer partner (SHP) were significantly elevated, along with the suppression of SREBP-1c and ChREBP, in BE-treated mice compared with those in mice in the HFD1 group (Figures 3G and 3H). The mRNA expression levels of genes downstream of SREBP-1c and ChREBP,

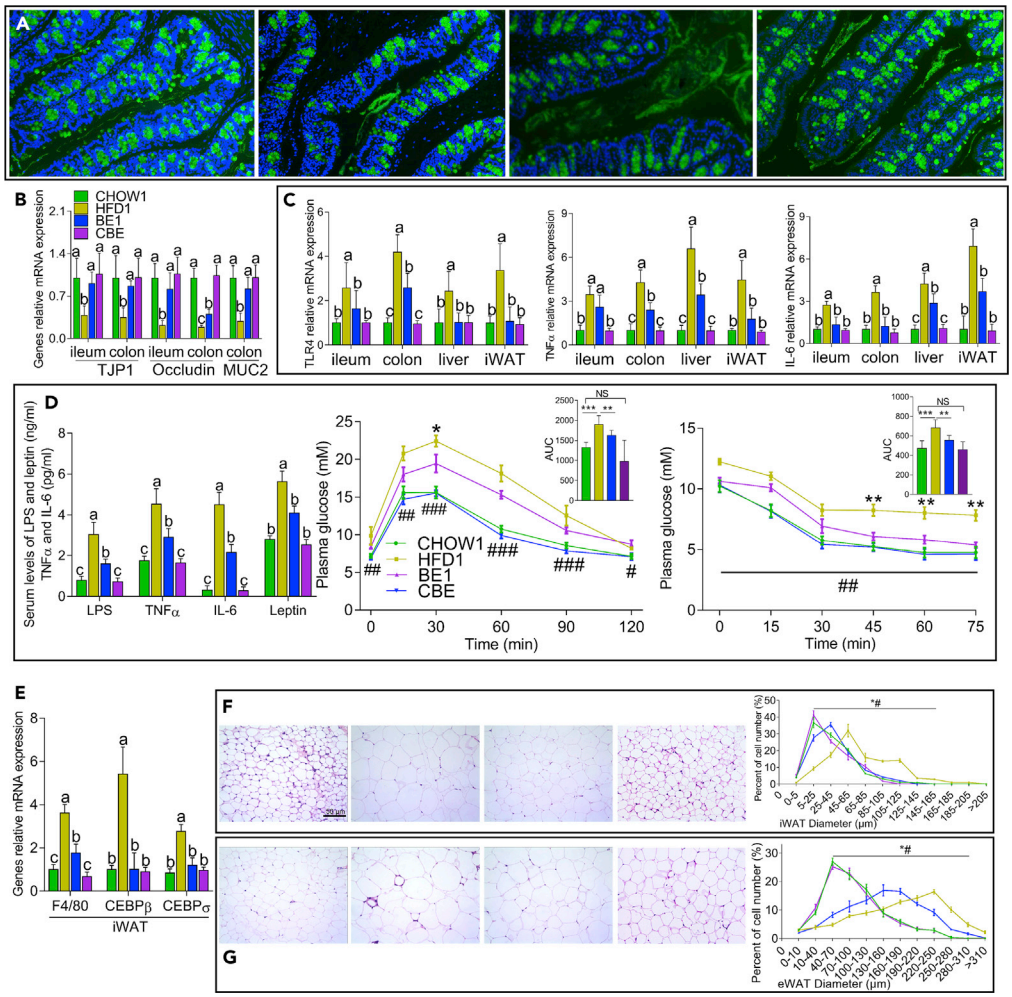

Figure 2. BE Treatment Ameliorated Systemic Inflammation and Improved Glucose Metabolism

(A) Fluorescence microscope analysis of colonic MUC2 in mice from the CHOW1, HFD1, BE1, and CBE groups (from left to right). MUC2, green; DNA, blue; n = 10.

(B and C) The relative mRNA expression of genes related to intestinal permeability (B) and inflammation (C).

(D) The serum contents of inflammatory factors and changes in blood glucose concentrations. *$p < 0.05$, **$p < 0.01$ and ***$p < 0.001$ for BE1 versus HFD1 and $^{\#}p < 0.05$, $^{\#\#}p < 0.01$, and $^{\#\#\#}p < 0.001$ for CHOW1 versus HFD1.

(E) The relative mRNA expression of genes in iWAT.

(F and G) Representative pictures showing the hematoxylin and eosin staining of iWAT (F) and eWAT (G) in CHOW1, HFD1, BE1, and CBE mice (from left to right) and the percentage of the cells with different diameters, *$p < 0.05$ for BE1 versus HFD1 and $^{\#}p < 0.05$ for CHOW1 versus HFD1. For all pictures, different letters indicate a significant difference between columns, $p < 0.05$.

including proliferator-activated receptor γ1 (PPARγ1), PPARγ2, fatty acid translocase (CD36), fatty acid synthase (FAS), glycerol-3-phosphate acyltransferase (GPAT), and fatty acid-binding protein 4 (FABP4), were all decreased in the livers of BE-treated mice compared with those of vehicle-treated HFD-fed mice (Figure 3G). Notably, there were strong correlations between the mRNA expression levels of FXRα, SHP, SREBP-1c, ChREBP, FAS, and CD36 (Figure 3G). In contrast, the mRNA levels of proteins related to lipolysis, including autophagy-related 4B cysteine peptidase (ATG4b), autophagy-related protein 5 (ATG5), ATG7, carnitine palmitoyltransferase (CPT-I), PPARα, and acetyl-coenzyme A synthetase (ACS), were increased in the livers of BE-treated mice compared with their levels in mice in the HFD1 group (Figure 3G). The expression of proteins related to lipid metabolism in WAT and brown adipose tissue (BAT) mirrored the results in the liver, except that FXRα and SHP were not influenced by BE (Figures S1A and 1B). Moreover, BE treatment reduced the mRNA expression of cytochrome P450 7A1 (CYP7A1), the key protein controlling BA synthesis, in the liver (Figure 3F), which was consistent with the reduced plasma BA pool size.

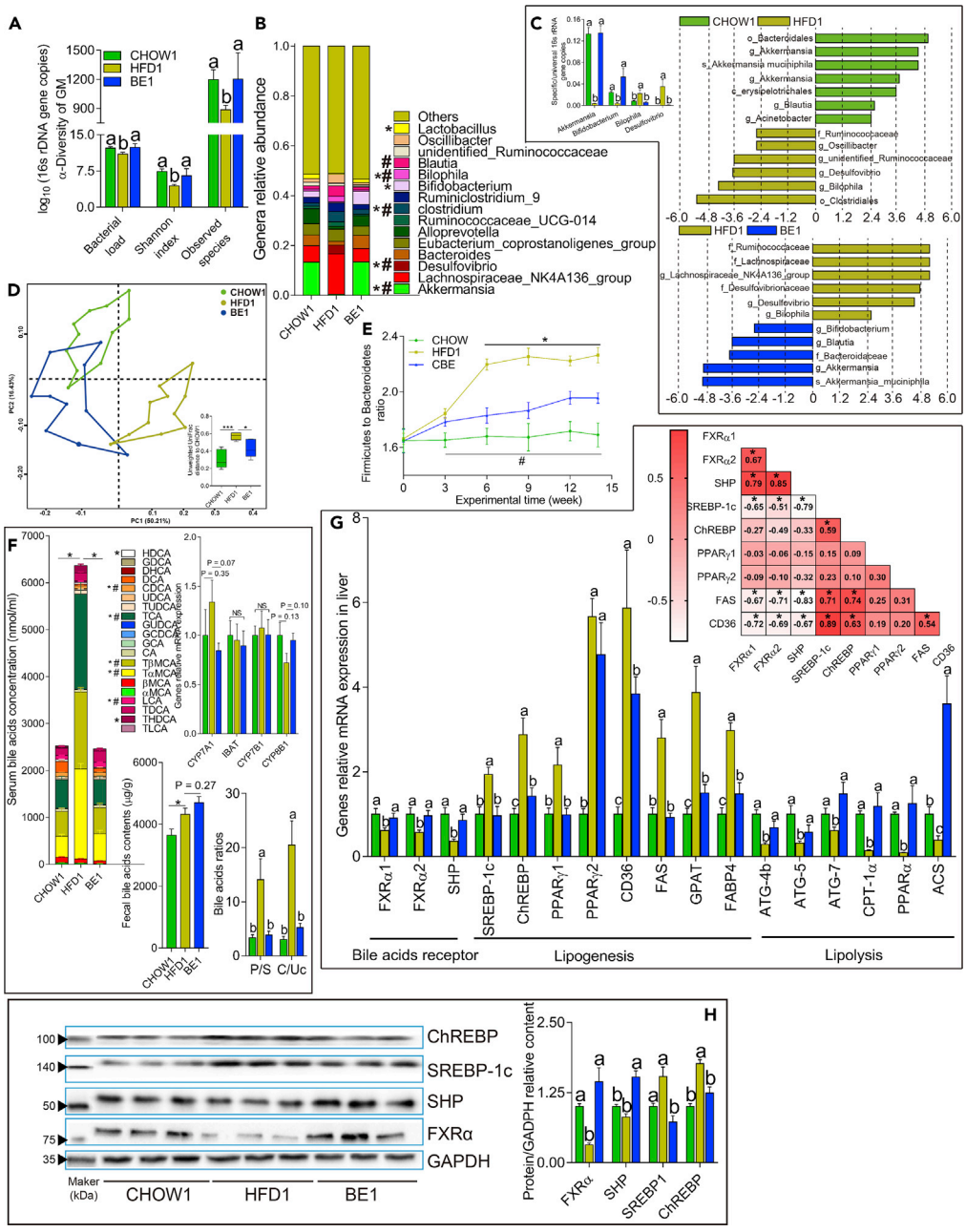

Figure 3. BE Administration Ameliorated the HFD-Induced Disturbance of the GM

(A) BE increased the α-diversity of the GM and the total bacterial load (based on 16S rRNA gene copies).

(B) Relative abundance of the top genera.

(C) The abundance of bacterial genera (left) identified by LEfSe analysis (right) in mice from the HFD1 and BE1 groups.

(D) Principal coordinate analysis (PCoA) of the GM based on the unweighted UniFrac distance.

(E) The alteration in the Firmicutes to Bacteroidetes ratio based on qPCR.

(F) BE administration changed the plasma BA pool size and composition (upper left) and the ratios of primary to secondary and conjugated to unconjugated BAs (bottom right), which was not related to the reabsorption or synthesis (upper right and bottom left) of BAs. P/S, primary BAs/secondary BAs; C/Uc, conjugated BAs/unconjugated BAs.

(G) The mRNA expression of genes related to lipid metabolism in the liver (bottom) and the correlation matrix between the mRNA expression levels of key genes controlling lipogenic and BA receptors (upper); r values and significance were according to Spearman's rank correlation test (*p < 0.05 if 0.362 < r < 0.467; *p < 0.01 if 0.467 < r < 0.580; *p < 0.001 if r > 0.580).

(H) Representative western blots showing the expression of proteins in the livers of mice from the CHOW1, HFD1, and BE1 groups (n = 3).

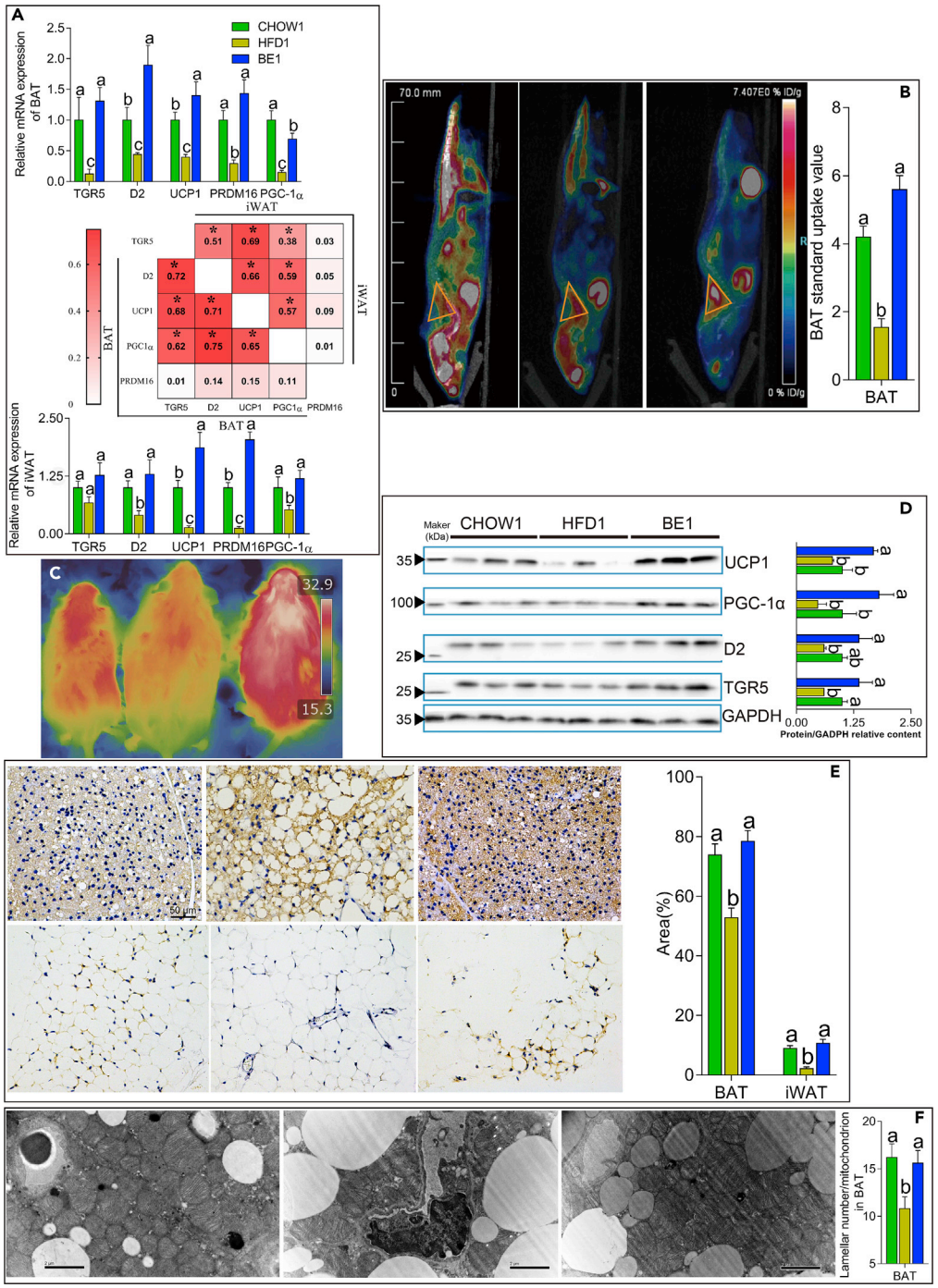

Figure 4. BE Administration Enhanced the Function of BAT and the Browning of iWAT

(A) The relative mRNA expression of genes related to the activation of BAT (up) and the browning of iWAT (down); correlation matrix between the mRNA expression of genes in BAT and iWAT (middle); r values and significance were according to Spearman's rank correlation test (*p < 0.05 if 0.362 < r < 0.467; *p < 0.01 if 0.467 < r < 0.580; *p < 0.001 if r > 0.580).

(B) Representative PET-CT scan of mice after mild cold stimulation. Yellow triangles indicate the anatomical site of the interscapular BAT, n = 5.

(C) Representative infrared thermal images, n = 8.

(D) Representative western blots showing the expression of proteins in BAT sections of mice from the CHOW1, HFD1, and BE1 groups (n = 3).

Figure 4. *Continued*

(E) Representative immunohistochemistry to detect UCP1 (brown stain) in BAT (upper left) and iWAT (bottom left) sections and the area under the curve AUC (right), n = 10.

(F) Representative transmission electronic microscopy images from BAT showing that BE treatment increased the lamellar cristae number in the mitochondria. Scale bar, 2 μm, original magnification 12,000×, n = 8. For (B, C, E, and F), the images represent mice from the CHOW1, HFD1, and BE1 groups from left to right. For all figures, different letters indicate a significant difference between columns, $p < 0.05$.

We then sought to determine the effect of BE on the activation of TGR5 in BAT. BE-treated mice showed elevated levels of the membrane BA receptor TGR5 and its downstream gene, deiodinase 2 (D2), in BAT (Figures 4A and 4D). Consistent with this, both the mRNA and protein expression of genes related to non-shivering thermogenesis (NST), including uncoupling protein-1 (UCP1), PR domain-containing 16 (PRDM16), and peroxisome proliferator-activated receptor gamma coactivator 1-alpha (PGC-1α), were increased in the BAT of BE-treated mice compared with their expression in vehicle-treated HFD-fed mice (Figures 4A, 4D, and 4E). There were strong positive correlations between the mRNA expression levels of TGR5, D2, UCP1, PGC-1α, and PRDM16 (Figure 4A). Consistent with these observations, we found significantly increased BAT functioning following cold stimulation through positron emission tomography-computed tomography (PET-CT) (Figure 4B) and an increased intrascapular temperature in BE-treated mice (Figure 4C), suggesting more powerful NST in the BAT of BE-treated mice. We also found more lamellar cristae in the mitochondria in the BAT of BE-treated mice than in the BAT of vehicle-treated HFD-fed mice (Figure 4F). In addition, our results also revealed a significant increase in the key proteins involved in the browning of adipocytes in iWAT, including D2, UCP1, PGC-1α, and PRDM16, although the mRNA expression of TGR5 ($p = 0.07$) was not significantly influenced by BE administration (Figures 4A and 4E). Collectively, these results suggested that BE administration promoted NST in BAT and the browning of iWAT through the BA membrane receptor TGR5, thereby increasing the energy expenditure and (in part) contributing to the anti-obesity effect of BE.

BE Improves Obesity and Its Related Metabolic Syndromes in *db/db* Mice by the Alteration of the GM and BAs

In mouse study 2, male C57BL/KsJ *db/db* mice purchased at 21 days of age were randomly assigned to two groups (n = 10) as follows: (1) a CHOW2 group fed a chow diet and (2) a BE2 group fed a chow diet with 5 gL^{-1} BE in drinking water. BE administration decreased genetically induced weight gain with no significant influence on the water consumption, energy intake, and energy in the feces, which was mainly the result of the decreased tissue weight of the liver, iWAT, and eWAT (Figure 5A). Liver steatosis, systemic inflammation, fat deposition and glucose metabolism were all improved by BE treatment (Figures 5A, 5C, S2, and S3A). BE-treated mice also had reduced serum TG, cholesterol, and leptin levels compared with mice in the CHOW2 group (Figure 5A). The improvement in adiposity was related to increased energy expenditure and an improvement in lipid metabolism (Figures 5B and S3A). BE-treated mice showed elevated mRNA expression of genes related to NST in iWAT and BAT and enhanced BAT functioning (Figures 5B–5E). There were strong correlations of the mRNA expression levels between TGR5, D2, PGC-1α, and PRDM16 and between FXR, SHP, SREBP-1c and ChREBP, suggesting that the regulation of lipid metabolism and enhancement of NST is closely linked to the activation of BA receptors FXR and TGR5 (Figures S3A and S3D).

BE administration increased the diversity of the GM, decreased the abundance of Proteobacteria and the ratio of Firmicutes to Bacteroidetes, and caused a significant difference in the GM of BE-treated mice compared with that of mice in the CHOW2 group, as based on the UniFrac distance (Figure 5D). Similar to the results of study 1, BE-treated mice had a lower level of plasma BAs, especially taurine-conjugated primary BAs (mainly TαMCA and TβMCA), and a higher ratio of secondary BAs (mainly LCA and CA) than control mice (Figure 5E). We did not observe differences in the fecal BA content or the mRNA expression in the IBAT between the mice in the two groups (Figure 5E), which was slightly different from the results of study 1. Moreover, there was a close correlation between the GM and plasma BA pool (Figure S1D). In summary, consistent with the results of study 1, BE administration improved genetically induced obesity and its related metabolic syndromes by the activation of TGR5 and FXR via the regulation of the GM and the plasma BA pool.

Antibiotic Treatment Blunts the Improvement in Metabolism by BE

Mouse study 3 was performed to determine whether there was a causal link between the regulation of the GM, the BA pool, and the improvement in metabolism upon BE administration. In this study, adult

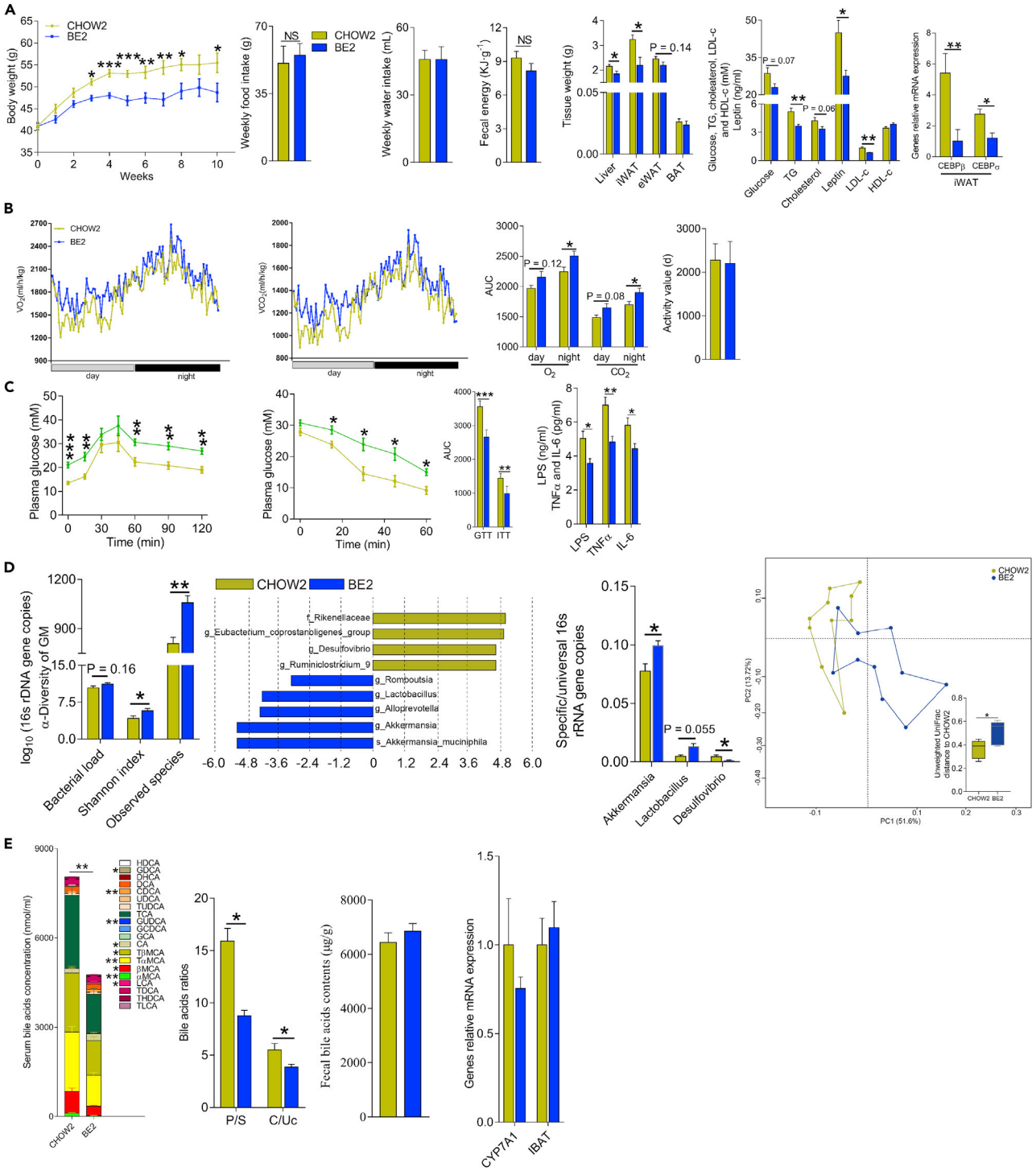

Figure 5. BE Treatment Improved Metabolic Syndromes by the Regulation of the BA Pool and the GM in *db/db* Mice

(A) The body weight (upper), food intake, water intake, fecal energy, tissue weights, plasma parameters, and gene expression (from left to right) of mice in study 2.

(B) Energy expenditure (left and middle) and physical activity (right) of mice.

(C) BE administration improved systemic inflammation (right), glucose intolerance (left and middle), and insulin resistance (middle).

(D) The α-diversity (left) and PCoA analysis of GM (right). The richness of certain bacterial genera identified by LEfSe (middle).

(E) Plasma BA composition (left and second from left), fecal BA contents (third from left), and the relative mRNA expression (right). For all figures, *$p < 0.05$, **$p < 0.01$, and ***$p < 0.001$.

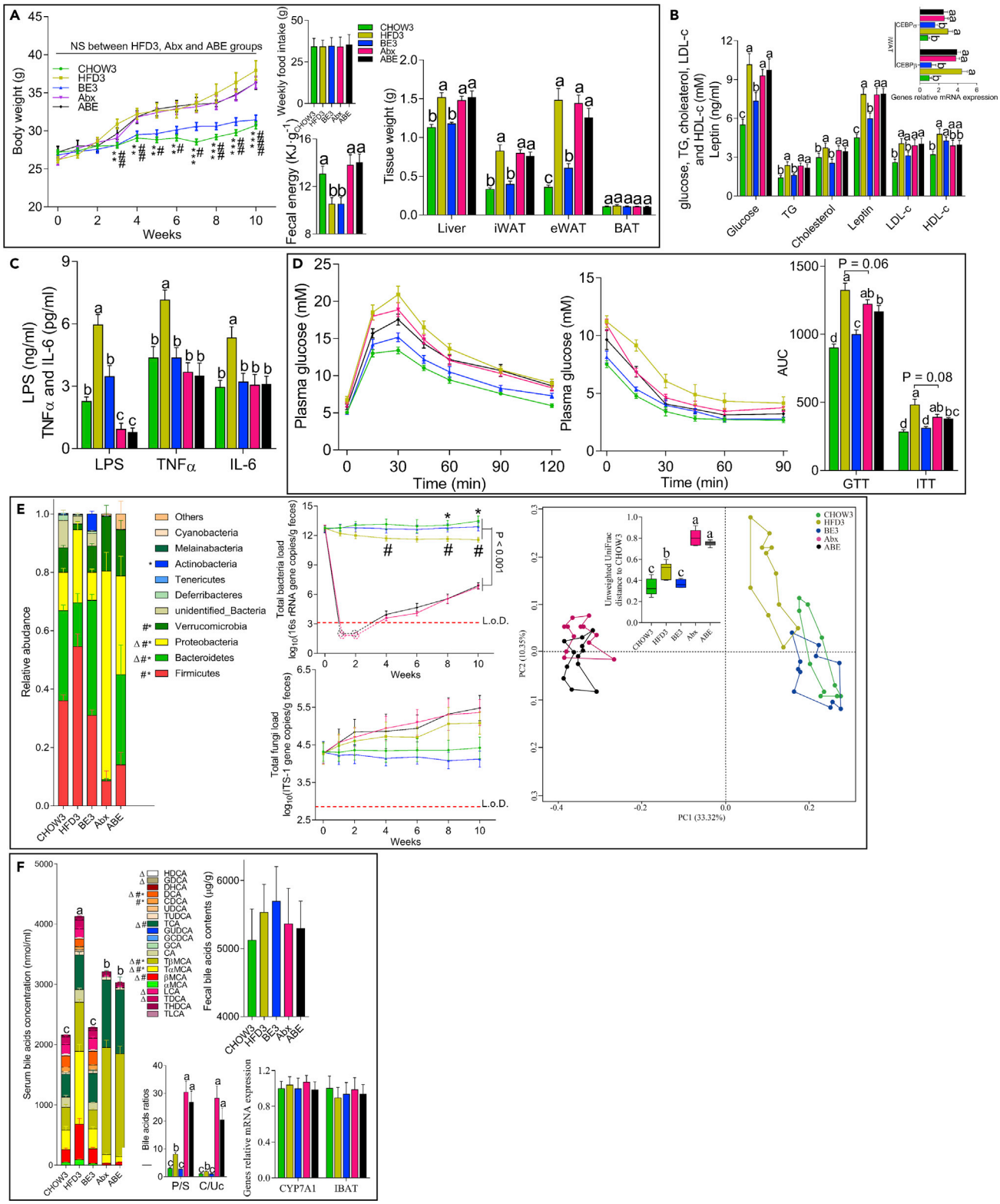

Figure 6. Antibiotic Treatment Blunted the Metabolic Improvement Effect in BE-Treated Mice

(A) Antibiotics blunted the anti-adiposis effect of BE (left and right), which was not related to energy intake or excretion (middle).

(B–D) There were no significant differences in serum parameters related to metabolic disease (B), systemic inflammation (C), and glucose metabolism (D) between mice in the Abx and ABE groups.

Figure 6. *Continued*

(E) Antibiotics substantially changed the composition of the GM (left and right) and decreased the abundance of gut bacteria (upper middle) but had no influence on the fungal richness (bottom middle). *p < 0.05 for HFD3 versus CHOW3, #p < 0.05 for HFD3 versus BE3, and $\Delta P < 0.05$ for HFD3 versus Abx/ABE. (F) Antibiotic treatment completely changed the plasma BA pool size and composition (left and bottom middle) but had no significant influence on the reabsorption or synthesis of BAs (bottom right) or the fecal concentration of BAs (upper right). *p < 0.05 for HFD3 versus CHOW3, #p < 0.05 for HFD3 versus BE3, and $\Delta P < 0.05$, for HFD3 versus Abx/ABE. For all figures, different letters indicate a significant difference between columns, p < 0.05.

(8-week-old) mice were used to minimize the side effects of antibiotics on metabolism as distribution of GM through antibiotics during early life time is strongly linked to various disorders such as obesity, type 1 diabetes, and allergy (Cox and Blaser, 2015; Livanos et al., 2016). Male C57BL/6 mice purchased at 49 days of age were randomly assigned to five groups (n = 10–12) as follows: (1) a CHOW3 group fed a chow diet, (2) an HFD3 group fed an HFD, (3) a BE3 group (5 gL^{-1} BE in drinking water) fed an HFD, (4) an Abx group fed an HFD, and (5) an ABE group (5 gL^{-1} BE in drinking water) fed an HFD. All the mice were gavaged daily with 200 μL PBS containing (for the Abx and ABE groups) 0.5 mg mL^{-1} ampicillin, 0.5 mg mL^{-1} gentamicin, 0.5 mg mL^{-1} metronidazole, 0.5 mg mL^{-1} neomycin, and 0.25 mg mL^{-1} vancomycin or no antibiotics (for the CHOW3, HFD3, and BE3 groups). Consistently, antibiotics had no significant influence on BW (Figure 6A), suggesting that the side effect of antibiotics on the BWs of adult mice was negligible. Antibiotics substantially reduced the gut bacteria to undetected levels during the first two weeks, whereas the abundance of fungi was not significantly influenced throughout the experiment (Figure 6E). Until the end of the experiment, the bacterial richness in antibiotic-treated mice was still quite low (approximately $10^7 \cdot g^{-1}$ feces), despite the increased tolerance to the antibiotics with time (Figure 6E). The fecal anthocyanin content was significantly higher in antibiotic-treated mice than in BE-treated antibiotic-free mice (Table S1), suggesting the impaired microbial degradation of anthocyanins. We also found that the GM of mice in the Abx and ABE groups was more similar than that of mice in the HFD and BE groups based on the unweighted UniFrac distance (Figure 6E). Antibiotic treatment sharply decreased the abundance of total, secondary, and free BAs compared with those in the antibiotic-free mice (Figure 6F). There was no significant difference in the plasma BA pool size and composition between mice in the Abx and ABE groups (Figure 6F). Taken together, these results suggest that antibiotics substantially blocked the interaction between BE and the GM, thereby destroying the regulation of the BA pool through the GM upon BE administration.

The disturbance of the regulation of the BA pool with antibiotic treatment blunted the activation of TGR5 and FXR through BE administration. There were no differences in the mRNA expression levels of FXR and TGR5 and their downstream genes SHP, SREBP-1c, ChREBP, D2, UCP1, PRDM16, and PGC-1α in the antibiotic- and antibiotic-BE-treated HFD-fed mice (Figure S6). Immunohistochemical analysis further showed that antibiotic-BE-treated mice exhibited similar protein expression of TGR5, D2, UCP1, FXR, SHP, and SREBP-1c as that of antibiotic- and vehicle-treated HFD-fed mice (Figure S7). The observations from PET-CT (data not shown), metabolic cage experiments, and transmission electron microscopy were consistent with these observations (Figure S4). Antibiotic-BE-treated mice had BWs, tissue weights, hepatic fat deposition, and serum TG and cholesterol contents similar to those of antibiotic- and vehicle-treated HFD-fed mice (Figures 6A, 6B, and S5). The improvement in glucose metabolism upon BE administration was partially but not fully counteracted by antibiotics, which may because of the improved inflammation upon antibiotics treatment (Figures 6C and 6D). Collectively, these data suggest that antibiotic treatment damaged the interaction between BE, the GM, and BAs; blunted the activation of TGR5 and FXR; and impaired the metabolic improvement effect of BE.

DCA and LCA Activate the TGR5 Pathway in Mouse Primary Adipocytes Derived from BAT, whereas TαMCA and TβMCA Inhibit the FXR Pathway in Mouse Primary Hepatocytes in a Dose-Dependent Manner

We then sought to determine whether these specific alterations in BAs *in vivo* could be reproduced *in vitro* using mouse primary adipocytes and hepatocytes derived from BAT and the liver, respectively. CDCA and LCA (3 μM) enhanced the expression of TGR5, D2, PGC-1α, and UCP1 in mouse primary adipocytes derived from BAT, and higher doses had a more significant influence (Figures 7C–7F). We next analyzed the effect of high levels of TαMCA and TβMCA on mouse primary hepatocytes with or without the presence of CDCA and found that CDCA increased the levels of FXR and SHP while suppressing the mRNA and protein expression of SREBP-1c and ChREBP (Figures 7A and 7B). The supplementation of TαMCA and TβMCA counteracted the effect of CDCA, and higher levels of TαMCA and TβMCA had a

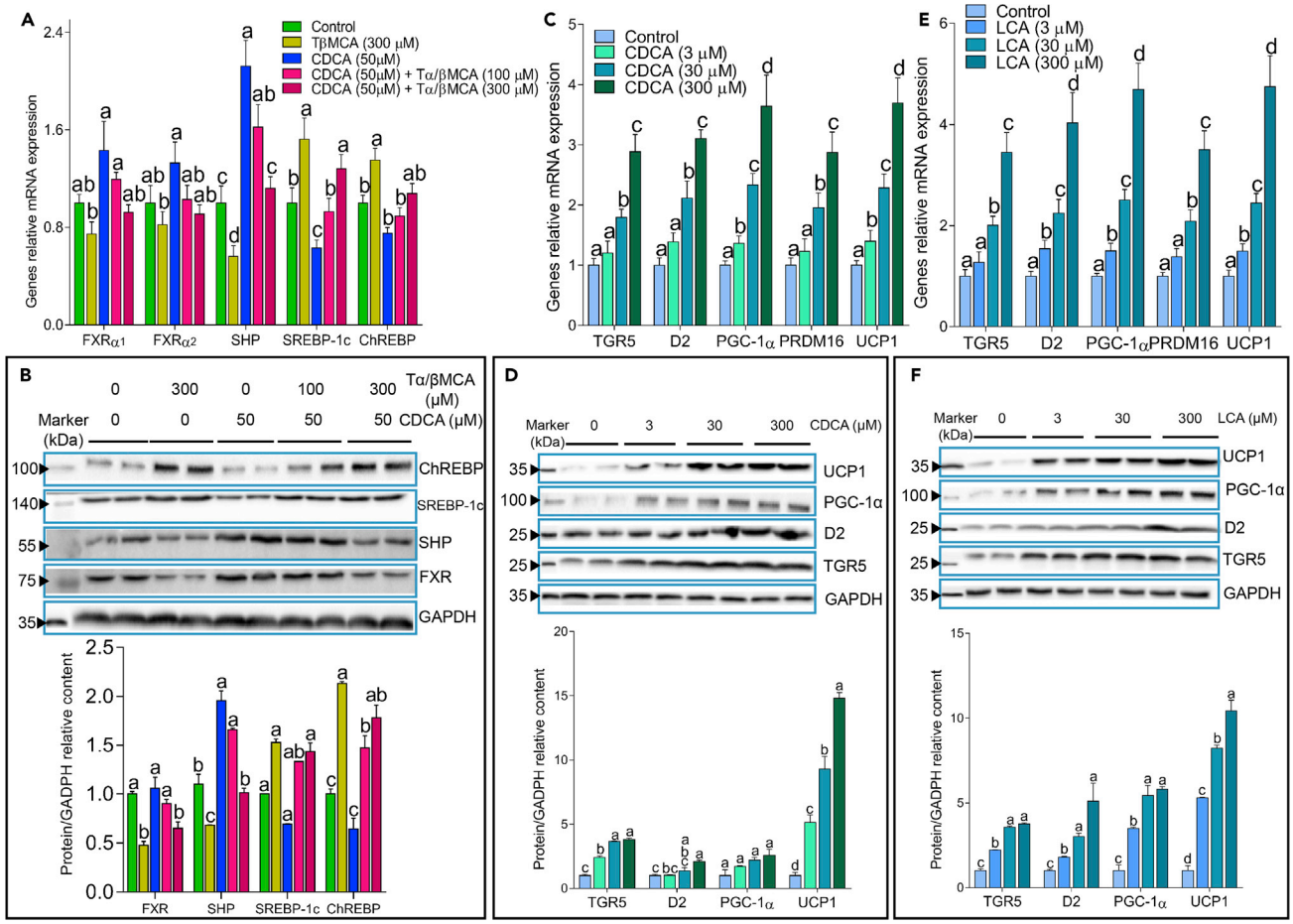

Figure 7. Tα/βMCA Suppressed the FXR Pathway, while CDCA and LCA Enhanced the TGR5 Pathway in Mouse Primary Cells

(A and B) Genes relative mRNA expression (A) and western blots (B) in mouse primary hepatocytes showed that CDCA enhanced the mRNA and protein expression of FXR and SHP while suppressing that of SREBP-1c and ChREBP, which was counteracted by Tα/βMCA treatment.

(C–F) Genes relative mRNA expression (C and E) and western blots (D and F) in mouse primary adipocytes derived from BAT showed that CDCA (C and D) and LCA (E and F) enhanced the mRNA and protein expression of TGR5 and its downstream genes related to thermogenesis; n = 2. For all images, different letters indicate a significant difference between columns, $p < 0.05$.

stronger effect, suggesting that TαMCA and TβMCA suppressed the activity of FXR and SHP in a dose-dependent manner (Figures 7A and 7B). Collectively, these results showed that the regulation of the plasma BA pool, mainly the reduction in TαMCA and TβMCA and the increase in secondary BAs (such as LCA and CDCA), through BE administration may have had a profound influence on mouse primary cells, which was in agreement with the results observed *in vivo* and may be responsible for the metabolic improvement effect of BE.

DISCUSSION

We established a possible pathway involving the GM and BAs to describe how the phenolic compounds in blueberries improve diet- and genetically induced adiposity and its related metabolic syndromes. The daily administration of BE strongly ameliorated the obesity-related disturbance of the GM, thereby regulating the abnormal plasma BA pool size and composition, which further activated the membrane and nuclear BA receptors TGR5 and FXR in BAT, iWAT, and the liver. The activation of TGR5 and FXR increased the energy expenditure in BAT, enhanced the browning of iWAT, and improved lipid metabolism in adipose tissues and the liver, therefore reducing adiposity and improving metabolic syndromes.

BE significantly influenced the abundance of various bacterial genera including *Akkermansia*, *Bifidobacterium*, *Lactobacillus*, and *Desulfovibrio*. *Bifidobacterium*, and *Lactobacillus*, which produce BSH, were positively

correlated with the increased concentration of plasma secondary and free BAs, such as CDCA, DCA, and LCA, and the ratio of secondary/primary BAs. A high ratio of secondary to primary BAs is linked to a decreased risk of non-alcoholic steatohepatitis and a healthy liver status (Molinaro et al., 2018). The high-level expression of BSH in the intestine resulted in reduced weight gain and plasma and hepatic TG concentrations in mice (Joyce et al., 2014), which is consistent with our observations. Although there was no direct evidence that *Akkermansia* produced BSH, *Akkermansia* abundance was correlated with the plasma BA pool, like the abundance of *Bifidobacteria* and *Lactobacillus*. The increase in *Akkermansia* was observed in Roux-en-Y gastric bypass (RYGB) surgery (Cox and Blaser, 2013), which was also associated with profound alteration of the BA pool (e.g., the reduction of taurine-conjugated BAs), the activation of FXR, significant metabolic improvement, and weight loss in the first week after surgery (Ryan et al., 2014; Li et al., 2011). Similar to RYGB, BE treatment ameliorated the HFD-induced increase in plasma taurine-conjugated BAs, including TαMCA and TβMCA, which are inhibitors of FXR and usually present in excess in obese individuals (Molinaro et al., 2018; Sayin et al., 2013), and activated the FXR in the liver. Activation of the FXR in the liver and mouse hepatocytes enhanced the expression of SHP, which further suppressed the activity of SREBP-1c (Watanabe et al., 2004) and its downstream genes related to lipid synthesis including ACC1, AP2, FAS, CD36, and GPAT. The supplementation of CA, an FXR agonist, also lowered TG levels through the activation of the FXR (Watanabe et al., 2004). BE treatment improved glucose metabolism in both wild-type and *db/db* mice, which seems to be related to the activation of the FXR in the liver because treatment of *db/db* mice with the FXR agonist GW4064 decreased hyperglycemia by suppressing the expression of PEPCK and G6Pase (Zhang et al., 2006). Taken together, these results suggest that the activation of the FXR, whether through the reduction of antagonist (RYGB and BE treatment) or the administration of agonist (CA), improved the metabolism in mice.

CA is also a moderate agonist of TGR5 (Perino and Schoonjans, 2015), and treating mice with CA prevented diet-induced obesity and IR (Watanabe et al., 2006). Other kinds of BAs, mainly LCA, DCA, and CDCA, are natural agonists of TGR5 and have effects similar to those of CA (Broeders et al., 2015). Our results showed that BE administration increased the abundance of these free BAs and that treating mouse primary adipocytes derived from BAT with these BAs activated TGR5 in a dose-dependent manner. The activation of TGR5 induces the intracellular accumulation of cyclic AMP, followed by the downstream activation of its signaling pathways, such as the activation of D2 (Thomas et al., 2008). D2 converts the prohormone thyroxine (T_4) to the active hormone triiodothyronine (T_3) and increases metabolic rates (Watanabe et al., 2006). Consistent with this, the activation of TGR5 enhanced the expression of a series of downstream genes related to energy expenditure of TGR5 including D2, UCP1, PRDM16, and PGC-1α both *in vivo* and *in vitro*. Antibiotic treatment dramatically decreased the richness of plasma secondary BAs compared with that in the antibiotic-free mice, and the BAT function of antibiotic-treated mice was also lower. However, this decreased BAT activity did not significantly influence BW, which may be because the extinction of the gut bacteria (that were capable of extracting energy from otherwise digested compounds in food) (Kundu et al., 2017) by antibiotics reduced the energy intake of mice from food, as indicated by the increased energy in the feces of antibiotic-treated mice. More importantly, BE administration had no significant effect on the BA pool and the activity of BAT in antibiotic-treated mice, suggesting that gut bacteria played a key role in BE functioning through BAT.

We also found that BE administration significantly reduced the abundance of *Desulfovibrio*, an important H_2S-producing bacteria in the intestine (Guo et al., 2018). Excess H_2S can reduce the disulfide bonds in the mucous network and increase the permeability of the intestine, thus contributing to the transposition of bacteria and their metabolites, such as LPS (Ijssennagger et al., 2016). This transposition is able to trigger an inflammatory response and induce IR (Cox et al., 2015). Therefore the reduction in *Desulfovibrio* may be partially conducive to the improvement of inflammation and glucose metabolism in BE-treated mice.

In summary, BE administration improved metabolism by reducing the FXR antagonist content and increasing the abundance of TGR5 agonists, which was fulfilled through regulation of the GM.

Limitations of the Study

The BE obtained from fresh blueberry fruit was a mixture that consisted of various kinds of phenolic compounds. Therefore, whether there is one or several key ingredients in BE and how BE influences the composition of the GM remains unclear. Moreover, further investigations on GM and BAs are needed to explore the underlying mechanisms of BE-GM-BA-metabolism axis. For example, a full analysis of the BA pools in the plasma, liver, gall bladder, and intestine and the determination of the expressions of BA-related genes would be very helpful to completely understand the influences on BA metabolism by BE treatment.

Similarly, sufficient analysis of GM employing metagenomic and metatranscriptomic approaches is also meaningful to have a comprehensive picture of GM alteration. Nevertheless, these results provide a new perspective on how dietary polyphenols function and show the importance of the interaction between the GM and dietary components.

METHODS

All methods can be found in the accompanying Transparent Methods supplemental file.

SUPPLEMENTAL INFORMATION

Supplemental Information can be found online at https://doi.org/10.1016/j.isci.2019.08.020.

ACKNOWLEDGMENTS

The work was supported by Research on Blueberry Functional Ingredients and the Development of New Blueberry Wine (201805410611582).

AUTHOR CONTRIBUTIONS

J.Z. and J.G. designed the study and wrote the manuscript. J.G., H.T., and X.H. performed the experiments. Y.Y. and W.H. contributed to the data analysis.

DECLARATION OF INTERESTS

The authors declare no competing interests.

Received: May 3, 2019
Revised: August 1, 2019
Accepted: August 12, 2019
Published: September 27, 2019

REFERENCES

Bäckhed, F., Ding, H., Wang, T., Hooper, L.V., Koh, G.Y., Nagy, A., Semenkovich, C.F., and Gordon, J.I. (2004). The gut microbiota as an environmental factor that regulates fat storage. Proc Natl Acad Sci U S A *101*, 15718.

Broeders, E.P., Nascimento, E.B., Havekes, B., Brans, B., Roumans, K.H., Tailleux, A., Schaart, G., Kouach, M., Charton, J., Deprez, B., et al. (2015). The bile acid chenodeoxycholic acid increases human Brown adipose tissue activity. Cell Metab. *22*, 418–426.

Cox, L.M., and Blaser, M.J. (2013). Pathways in microbe-induced obesity. Cell Metab. *17*, 883–894.

Cox, L.M., and Blaser, M.J. (2015). Antibiotics in early life and obesity. Nat. Rev. Endocrinol. *11*, 182–190.

Cox, A.J., West, N.P., and Cripps, A.W. (2015). Obesity, inflammation, and the gut microbiota. Lancet Diabetes Endocrinol. *3*, 207–215.

Defuria, J., Bennett, G., Strissel, K.J., Perfield, J.W., II, Milbury, P.E., Greenberg, A.S., and Obin, M.S. (2009). Dietary blueberry attenuates whole-body insulin resistance in high fat-fed mice by reducing adipocyte death and its inflammatory sequelae. J. Nutr. *139*, 1510–1516.

Friedman, J.M., and Halaas, J.L. (1998). Leptin and the regulation of body weight in mammals. Nature *395*, 763–770.

Gerard, P. (2013). Metabolism of cholesterol and bile acids by the gut microbiota. Pathogens *3*, 14–24.

Gregor, M.F., and Hotamisligil, G.S. (2011). Inflammatory mechanisms in obesity. Annu. Rev. Immunol. *29*, 415–445.

Guo, J.L., Han, X., Zhan, J.C., You, Y.L., and Huang, W.D. (2018). Vanillin alleviates high fat diet-induced obesity and improves the gut microbiota composition. Front. Microbiol. *9*, 2733.

Han, X., Guo, J., You, Y., Yin, M., Liang, J., Ren, C., Zhan, J., and Huang, W. (2018). Vanillic acid activates thermogenesis in brown and white adipose tissue. Food Funct. *9*, 4366.

Hanhineva, K., Torronen, R., Bondia-Pons, I., Pekkinen, J., Kolehmainen, M., Mykkanen, H., and Poutanen, K. (2010). Impact of dietary polyphenols on carbohydrate metabolism. Int. J. Mol. Sci. *11*, 1365–1402.

Ijssennagger, N., Van Der Meer, R., and Van Mil, S.W.C. (2016). Sulfide as a mucus barrier-breaker in inflammatory bowel disease? Trends Mol. Med. *22*, 190–199.

Joyce, S.A., Macsharry, J., Casey, P.G., Kinsella, M., Murphy, E.F., Shanahan, F., Hill, C., and Gahan, C.G. (2014). Regulation of host weight gain and lipid metabolism by bacterial bile acid modification in the gut. Proc. Natl. Acad. Sci. U S A *111*, 7421–7426.

Just, S., Mondot, S., Ecker, J., Wegner, K., Rath, E., Gau, L., Streidl, T., Hery-Arnaud, G., Schmidt, S., Lesker, T.R., et al. (2018). The gut microbiota drives the impact of bile acids and fat source in diet on mouse metabolism. Microbiome *6*, 134.

Kastorini, C.M., Milionis, H.J., Esposito, K., Giugliano, D., Goudevenos, J.A., and Panagiotakos, D.B. (2011). The effect of Mediterranean diet on metabolic syndrome and its components: a meta-analysis of 50 studies and 534,906 individuals. J. Am. Coll. Cardiol. *57*, 1299–1313.

Kay, C.D., Pereira-Caro, G., Ludwig, I.A., Clifford, M.N., and Crozier, A. (2017). Anthocyanins and flavanones are more bioavailable than previously perceived: a review of recent evidence. Annu. Rev. Food Sci. Technol. *8*, 155–180.

Kundu, P., Blacher, E., Elinav, E., and Pettersson, S. (2017). Our gut microbiome: the evolving inner self. Cell *171*, 1481–1493.

Lee, S., Keirsey, K.I., Kirkland, R., Grunewald, Z.I., Fischer, J.G., and De, C.L.S. (2018). Blueberry supplementation influences the gut microbiota, inflammation, and insulin resistance in high-fat-diet-fed rats. J. Nutr. *148*, 209.

Li, J.V., Ashrafian, H., Bueter, M., Kinross, J., Sands, C., Le Roux, C.W., Bloom, S.R., Darzi, A., Athanasiou, T., et al. (2011). Metabolic surgery profoundly influences gut microbial-host metabolic cross-talk. Gut *60*, 1214–1223.

Livanos, A.E., Greiner, T.U., Vangay, P., Pathmasiri, W., Stewart, D., Mcritchie, S., Li, H., Chung, J., Sohn, J., Kim, S., et al. (2016). Antibiotic-mediated gut microbiome perturbation accelerates development of type 1 diabetes in mice. Nat. Microbiol. *1*, 16140.

Molinaro, A., Wahlstrom, A., and Marschall, H.U. (2018). Role of bile acids in metabolic control. Trends Endocrinol. Metab. *29*, 31–41.

Neto, C.C. (2010). Cranberry and blueberry: evidence for protective effects against cancer and vascular diseases. Mol. Nutr. Food Res. *51*, 652–664.

Perino, A., and Schoonjans, K. (2015). TGR5 and immunometabolism: insights from physiology and pharmacology. Trends Pharmacol. Sci. *36*, 847–857.

Ridaura, V.K., Faith, J.J., Rey, F.E., Cheng, J., Duncan, A.E., Kau, A.L., Griffin, N.W., Lombard, V., Henrissat, B., Bain, J.R., et al. (2013). Gut microbiota from twins discordant for obesity modulate metabolism in mice. Science *341*, 1241214.

Ryan, K.K., Tremaroli, V., Clemmensen, C., Kovatcheva-Datchary, P., Myronovych, A., Karns, R., Wilson-Perez, H.E., Sandoval, D.A., Kohli, R., Backhed, F., and Seeley, R.J. (2014). FXR is a molecular target for the effects of vertical sleeve gastrectomy. Nature *509*, 183–188.

Sayin, S.I., Wahlstrom, A., Felin, J., Jantti, S., Marschall, H.U., Bamberg, K., Angelin, B., Hyotylainen, T., Oresic, M., and Backhed, F. (2013). Gut microbiota regulates bile acid metabolism by reducing the levels of tauro-beta-muricholic acid, a naturally occurring FXR antagonist. Cell Metab. *17*, 225–235.

Stull, A.J., Cash, K.C., Johnson, W.D., Champagne, C.M., and Cefalu, W.T. (2010). Bioactives in blueberries improve insulin sensitivity in obese, insulin-resistant men and women. J. Nutr. *140*, 1764–1768.

Swann, J.R., Want, E.J., Geier, F.M., Spagou, K., Wilson, I.D., Sidaway, J.E., Nicholson, J.K., and Holmes, E. (2011). Systemic gut microbial modulation of bile acid metabolism in host tissue compartments. Proc. Natl. Acad. Sci. U S A *108 Suppl 1*, 4523–4530.

Thomas, C., Pellicciari, R., Pruzanski, M., Auwerx, J., and Schoonjans, K. (2008). Targeting bile-acid signalling for metabolic diseases. Nat. Rev. Drug Discov. *7*, 678–693.

Tresserra-Rimbau, A., Medina-Remon, A., Lamuela-Raventos, R.M., Bullo, M., Salas-Salvado, J., Corella, D., Fito, M., Gea, A., Gomez-Gracia, E., Lapetra, J., et al. (2015). Moderate red wine consumption is associated with a lower prevalence of the metabolic syndrome in the PREDIMED population. Br. J. Nutr. *113* (*Suppl 2*), S121–S130.

Turnbaugh, P.J., Ley, R.E., Mahowald, M.A., Magrini, V., Mardis, E.R., and Gordon, J.I. (2006). An obesity-associated gut microbiome with increased capacity for energy harvest. Nature *444*, 1027–1031.

Watanabe, M., Houten, S.M., Wang, L., Moschetta, A., Mangelsdorf, D.J., Heyman, R.A., Moore, D.D., and Auwerx, J. (2004). Bile acids lower triglyceride levels via a pathway involving FXR, SHP, and SREBP-1c. J. Clin. Invest. *113*, 1408–1418.

Watanabe, M., Houten, S.M., Mataki, C., Christoffolete, M.A., Kim, B.W., Sato, H., Messaddeq, N., Harney, J.W., Ezaki, O., Kodama, T., et al. (2006). Bile acids induce energy expenditure by promoting intracellular thyroid hormone activation. Nature *439*, 484–489.

Zhang, Y.Q., Lee, F.Y., Barrera, G., Lee, H., Vales, C., Gonzalez, F.J., Willson, T.M., and Edwards, P.A. (2006). Activation of the nuclear receptor FXR improves hyperglycemia and hyperlipidemia in diabetic mice. Proc Natl Acad Sci U S A *103*, 1006–1011.

ISCI, Volume *19*

Supplemental Information

Blueberry Extract Improves Obesity through Regulation of the Gut Microbiota and Bile Acids via Pathways Involving FXR and TGR5

Jielong Guo, Xue Han, Hongyu Tan, Weidong Huang, Yilin You, and Jicheng Zhan

Table S1 Composition of BE and fecal anthocyanins, related to Figure 1 to Figure 6.

		Extract content (mg/g BE)
	Sugar	15.2 ± 1.23
	Protein	11.0 ± 1.09
	Lipid	2.82 ± 0.23
	Water	76.9 ± 6.10
	Total polyphenols	796.15 ± 36.41
	Unkown	97.60 ± 12.10
Anthocyanins	Total	219.24 ± 23.26
	Cyanidin-3-hexosides	13.31 ± 0.81
	Delphinidin-3-hexosides	56.77 ± 5.63
	Petunidin-3-hexosides	36.73 ± 2.59
	Malvidin-3-hexosides	60.9 ± 5.52
Proanthocyanidins		161.8 ± 23.85
Phenolic acids	Total	77.91 ± 9.82
	caffeic acid	2.37 ± 0.34
	p-Coumaric acid	13.52 ± 1.28
	Ferulic Acid	10.08 ± 1.17
	4-Hydroxybenzoic acid	21.99 ± 2.38
	Gallic acid	6.83 ± 0.91
	Protocatechuic acid	6.75 ± 0.84
	Vanillic acid	7.87 ± 0.92
Flavanols/flavonols	Total	101.88 ± 12.46
	Quercetin-3-hexosides	37.04 ± 5.93
	Myricetin-hexosides	48.91 ± 5.82
	Kaempferol-hexosides	6.79 ± 0.81

Fecal anthocyanins contents (mg/g)

mg/g feces	Cyanidin-3-hexosides	Delphinidin-3-hexosides	Petunidin-3-hexosides	Malvidin-3-hexosides	Total
BE1	ND	0.27 ± 0.12[a]	0.19 ± 0.11[a]	0.29 ± 0.17[a]	0.75 ± 0.37[a]
BE2	0.19 ± 0.13[a]	0.31 ± 0.15[a]	0.26 ± 0.17[a]	0.24 ± 0.13[a]	1.00 ± 0.42[a]
BE3	0.14 ± 0.08[a]	0.34 ± 0.13[a]	ND	0.33 ± 0.19[a]	0.82 ± 0.31[a]
ABE	1.09 ± 0.58[b]	2.49 ± 1.21[b]	1.51 ± 1.36[b]	2.33 ± 1.91[b]	7.42 ± 2.09[b]

Data are presented as the mean ± SD.

Hexosides represent glucoside, galactoside and arabinoside.

Data labeled with different letters have significant difference, $P < 0.05$.

Table S2 Diet composition, related to Figure 1 to Figure 6.

	D12450B		**D12492**	
	gm%	*kcal%*	gm%	*kcal%*
Protein	19.2	*20*	26.2	*20*
Carbohydrate	67.3	*70*	26.3	*20.1*
Fat	4.3	*10*	34.9	*59.9*
Total		*100*		*100*
kcal/gm	3.85		5.24	
Ingredient	**gm**	***kcal***	**gm**	***kcal***
Casein	200	*800*	200	*800*
L-Cystine	3	*12*	3	*12*
Corn Starch	315	*1260*	0	*0*
Maltodextrin 10	35	*140*	125	*500*
Sucrose	350	*1400*	68.8	*275.2*
Cellulose, BW200	50	*0*	50	*0*
Soybean Oil	25	*225*	25	*225*
Lard	20	*180*	245	*2205*
Mineral Mix S10026	10	*0*	10	*0*
DiCalcium Phosphate	13	*0*	13	*0*
Calcium Carbonate	5.5	*0*	5.5	*0*
Potassium Citrate, 1 H2O	16.5	*0*	16.5	*0*
Vitamin Mix V10001	10	*40*	10	*40*
Choline Bitartrate	2	*0*	2	*0*
FD&C Yellow Dye #5	0.05	*0*	0	*0*
FD&C Red Dye #40	0	*0*	0	*0*
FD&C Blue Dye #1	0	*0*	0.05	*0*
Total	**1055.05**	***4057***	**773.85**	***4057***

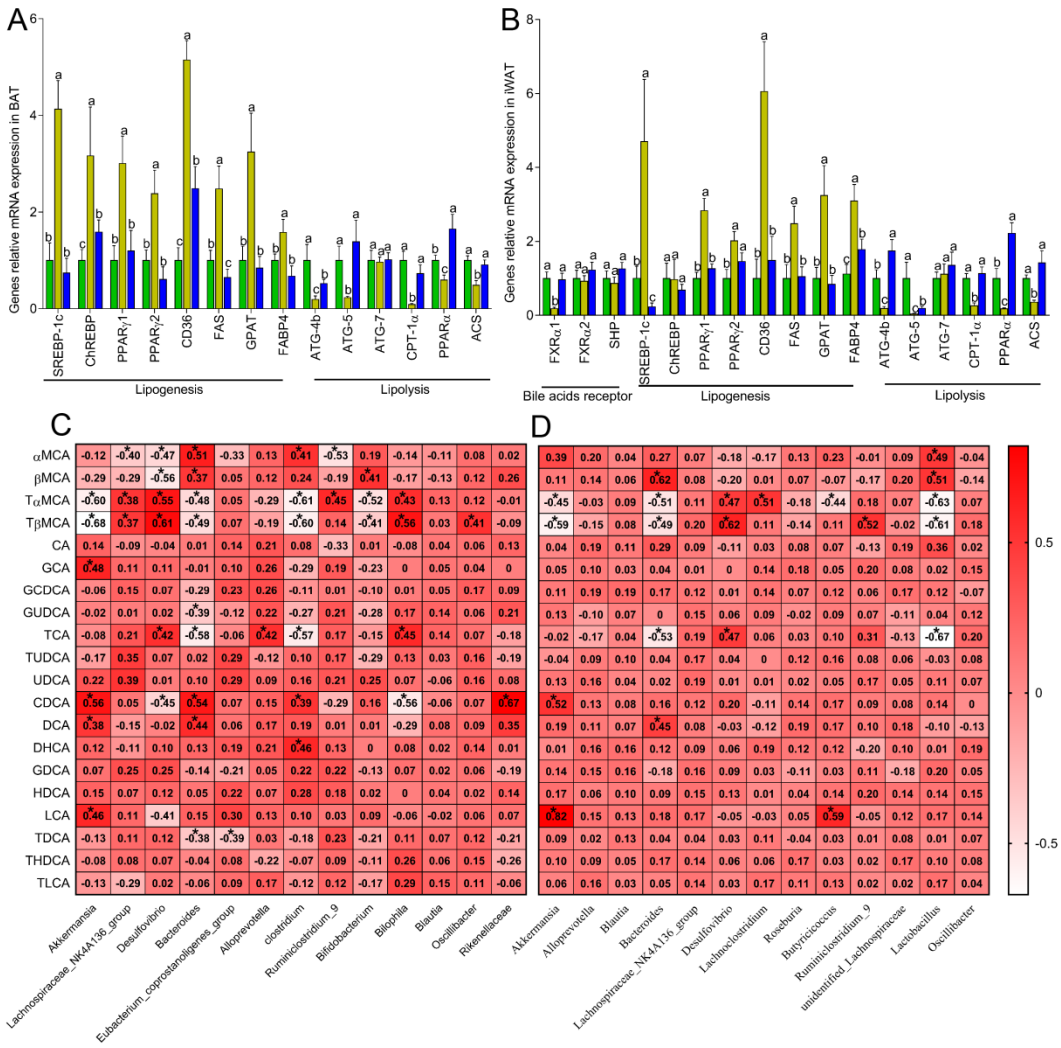

Figure S1 BE administration improved lipid metabolism in BAT and iWAT and the correlation heatmap between the most abundant bacterial genera and the plasma bile acids, related to Figure 3 and 5. The relative mRNA expression of genes in BAT (**A**) and iWAT (**B**) showed that BE administration suppressed the lipogenesis while enhanced lipolysis in BAT and iWAT. Correlation heatmaps between the most abundant bacteria taxa and the plasma bile acids of mice from study1 (**C**) and study2 (**D**) showed that there were strong correlations exiting. Significance and r values were according to Spearman (*$P < 0.05$* if 0.362 < r < 0.467; *$P < 0.01$* if 0.467 < r < 0.580; *$P < 0.001$* if r > 0.580 for (**C**) and *$P < 0.05$* if 0.435 < r < 0.556; *$P < 0.01$* if 0.556 < r < 0.681; *$P < 0.001$* if r > 0.681 for (**D**)).

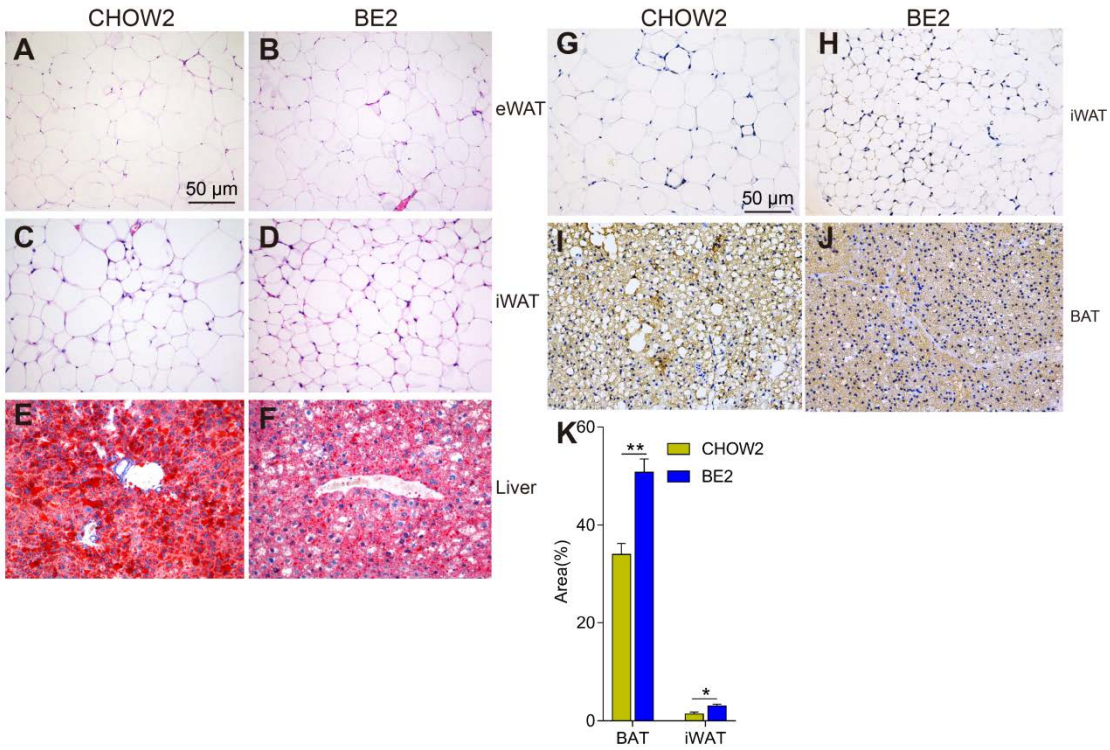

Figure S2 BE treatment decreased the fat deposition in WAT and liver, related to Figure 5. (**A**–**D**) Representative H&E staining of eWAT and iWAT of mice from CHOW2 and BE2 groups showed that BE treatment reduced fat deposition in WAT as well as the size of adipocytes, n = 10. (**E** and **F**) Representative oil red O staining of liver of mice from CHOW2 and BE2 groups, red areas indicate the lipid, n = 10. BE treatment enhanced the browning of iWAT (**G** and **H**) and the expression of UCP1 in BAT (**I** and **J**). (**K**) Area percent of the stained parts.

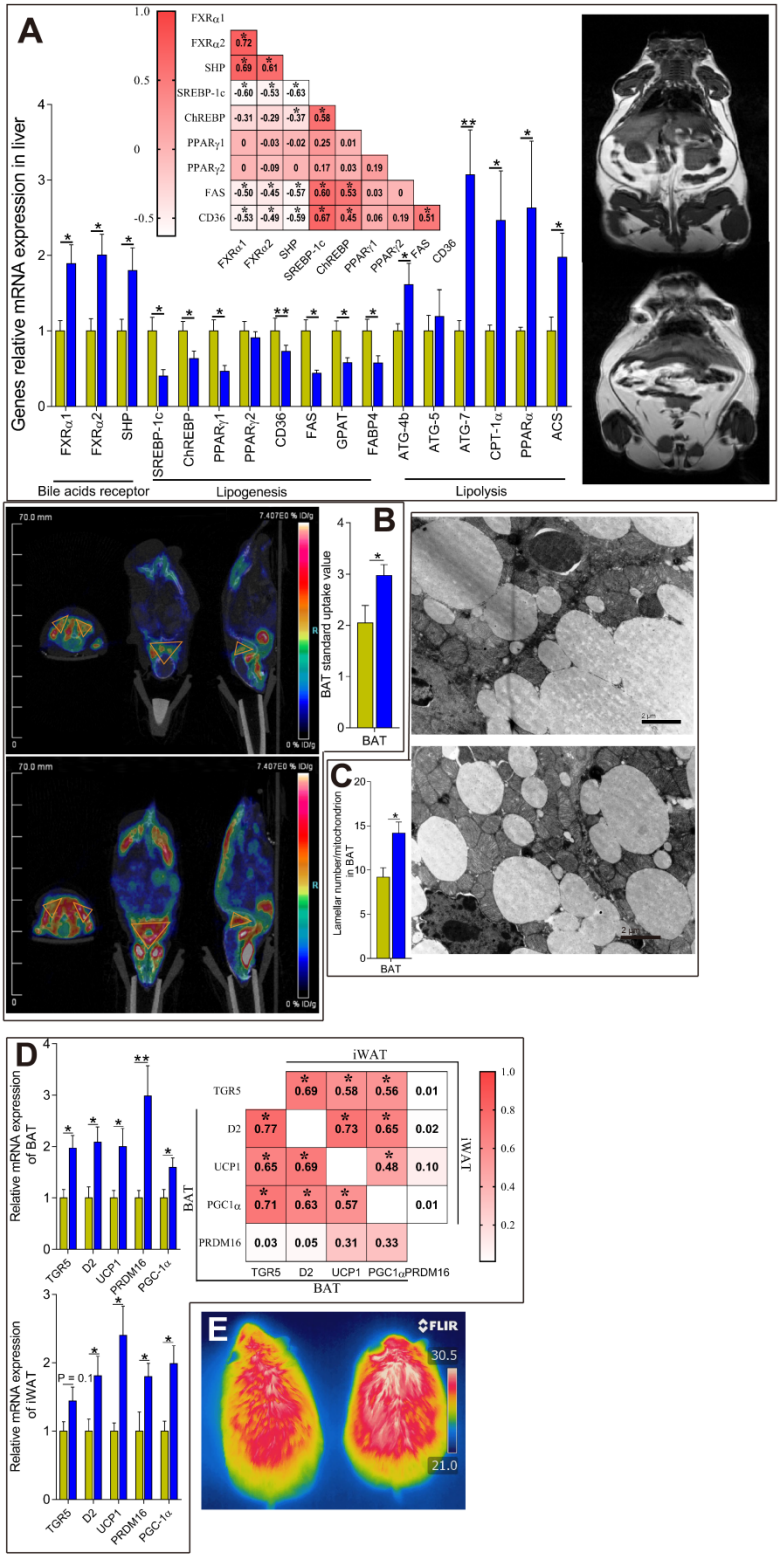

Figure S3 BE administration improves genetically-induced obesity and enhanced energy expenditure of *db/db* mice, related to Figure 5. (**A**) The relative mRNA expression of genes in liver (left bottom) and representative MRI images (right) (upper, CHOW2; lower, BE2); white areas indicate lipids, n = 8. Upper left, correlation matrix between the mRNA expression levels of key genes controlling lipogenic and BA receptors;

r values and significance were according to Spearman's rank correlation test (*$P < 0.05$* if 0.435 < r < 0.556; *$P < 0.01$* if 0.556 < r < 0.681; *$P < 0.001$* if r > 0.681). (**B**) Representative PET/CT scan (upper left, CHOW2; lower left, BE2) of mice after mild cold stimulation. Yellow triangles indicate the anatomical site of the interscapular BAT, n = 5. (**C**) Representative transmission electronic microscopy images (upper right, CHOW2; lower right, BE2) of BAT. Scale bar, 2 μm, original magnification 12,000×, n = 8. (**D**) The mRNA expression of genes related to the activation of BAT (upper left) and the browning of iWAT (bottom left). Right, correlation matrix between the mRNA expression of genes in BAT and iWAT; r value and significance were according to Spearman's rank correlation test (*$P < 0.05$* if 0.435 < r < 0.556; *$P < 0.01$* if 0.556 < r < 0.681; *$P < 0.001$* if r > 0.681). (**E**) Representative infrared thermal images of mice in BE2 (right) and CHOW2 groups (left). For all figures, *$P < 0.05$*, **$P < 0.01$* and ***$P < 0.001$*.

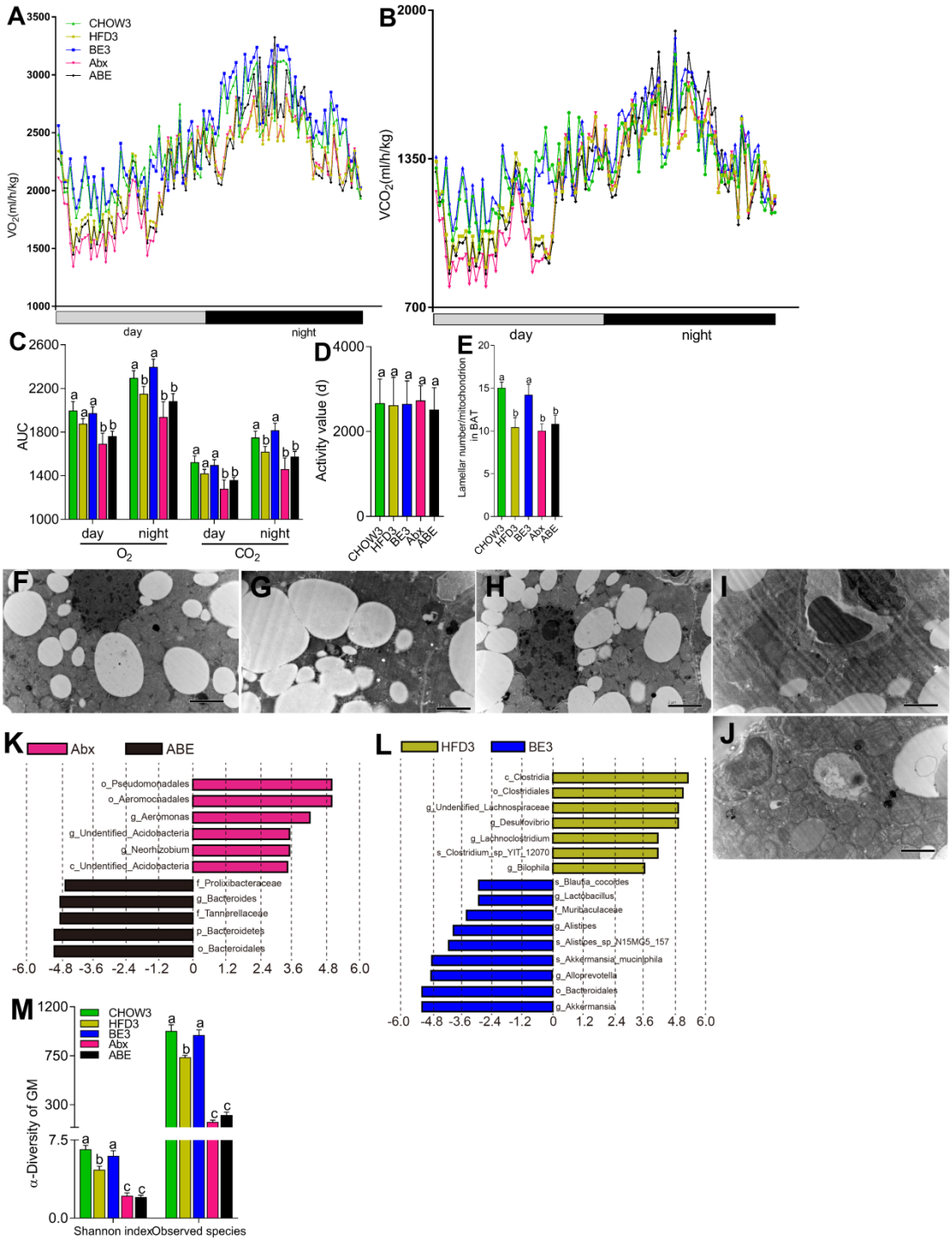

Figure S4 **Antibiotics treatment blunted the increase of energy expenditure and the regulation of GM in BE-treated mice, related to Figure 6**. (**A**, **B** and **C**) The daily O_2 consumption (**A**), CO_2 production (**B**) of mice and the relative AUC (**C**). Columns indicated with different letters have significant difference, *P < 0.05*. (**D**) The daily activity of mice showed that the discrepancy on energy expenditure was not related to the physical activity. (**F**-**J**) Representative transmission electron microscope images of mitochondria in BAT of mice belong to CHOW3, HFD3, BE3, Abx and ABE groups, respectively. (**E**) Quantification of the lamellar number in BAT, n = 9-12. (**K** and **I**) Biomarkers identified by

LEfSe between Abx and ABE (**K**), HFD3 and BE3 (**I**) groups. (**M**) The Shannon index and observed species of GM. For all pictures, columns indicated with different letters have significant difference, $P < 0.05$.

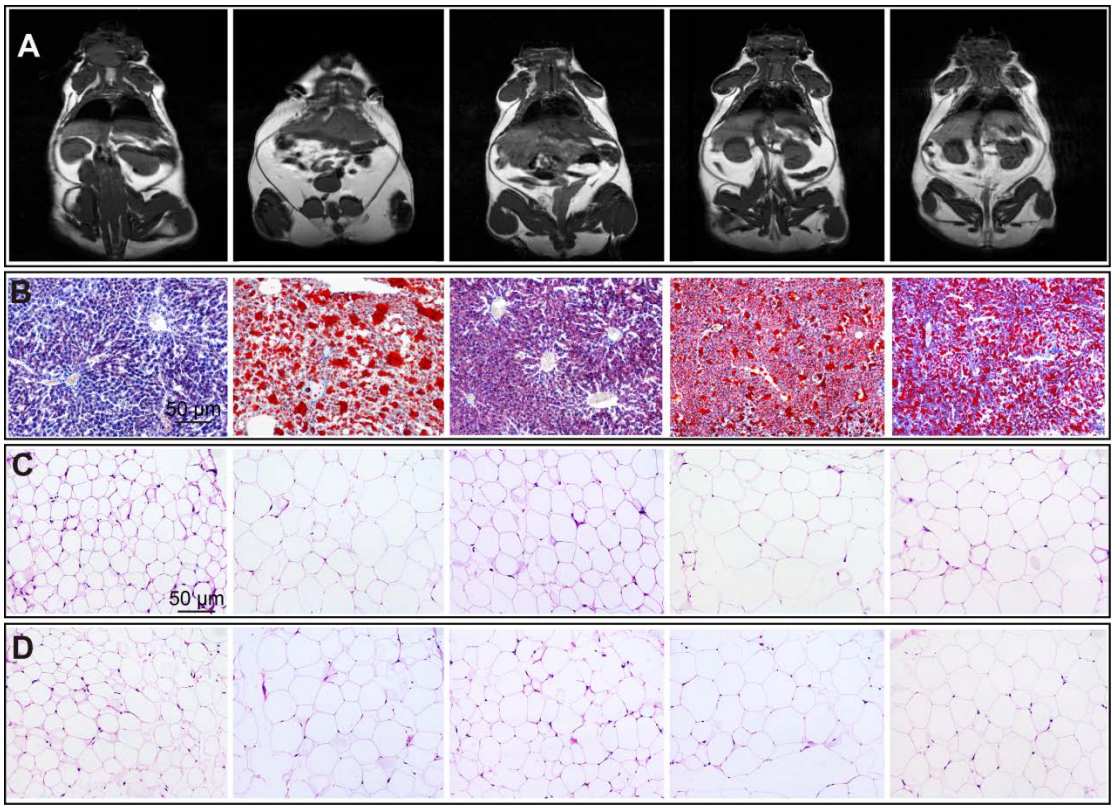

Figure S5 Antibiotics blunted the improvement of adiposity and fat deposition in liver and WAT upon BE administration, related to Figure 6. (**A**) Representative MRI images, white part represent the lipid. (**B**) Representative oil red O staining images of liver, red part represent the lipid. (C) Representative H&E staining images of eWAT. (**D**) Representative H&E staining images of iWAT. For all treatments, images represent the mice of CHOW3, HFD3, BE3, Abx and ABE groups, respectively, from left to right, n = 9 – 12.

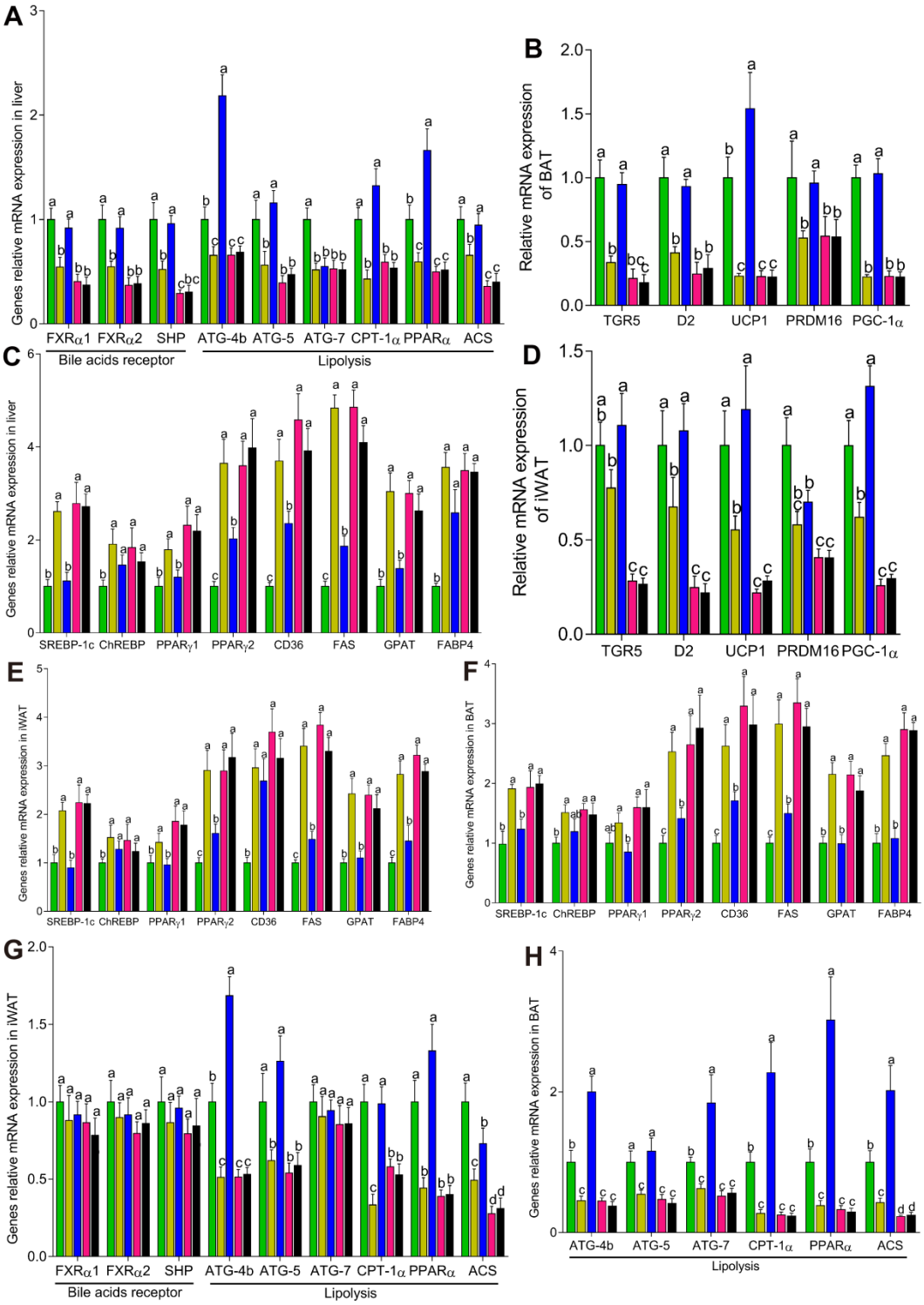

Figure S6 Antibiotics treatment totally blunted the metabolic regulation effect of BE in liver, iWAT and BAT, related to Figure 6. (**A**, **C and E-H**) BE administration enhanced the mRNA expression of FXR and SHP, elevated the mRNA expression of genes related with lipolysis (**A**) and suppressed the mRNA expression of SREBP-1c and its' downstream genes related to lipogenesis in liver (**A**), which were totally blunted by antibiotics treatment and similar results were observed in iWAT (**E** and **G**) and BAT (**F** and **H**). (**B** and **D**) The enhancement of the activation of BAT and the browning of iWAT in BE treated mice were

blunted by antibiotics treatment. For all pictures, columns indicated with different letters have significant difference, $P < 0.05$.

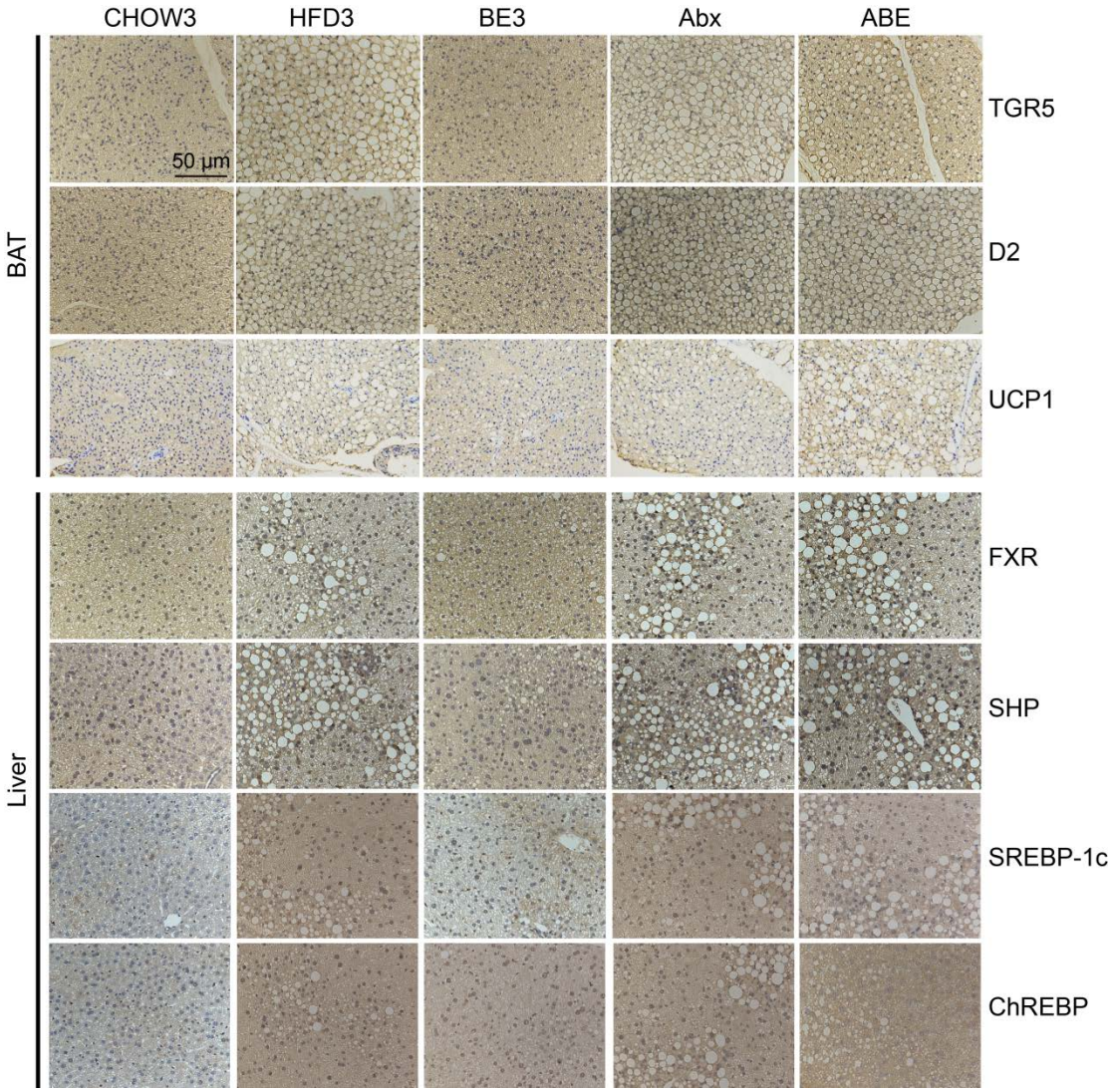

Figure S7 Antibiotics treatment blunted the regulation of protein expression related to NST in BAT and lipogenesis in liver, related to Figure 6. Representative immunohistochemistry images for proteins related to NST in BAT and lipogenesis in liver showed that BE administration enhanced NST and suppressed lipogenesis, which were blunted by antibiotics treatment, n=9-12

Methods

KEY RESOURCES TABLE

REAGENT or RESOURCE	SOURCE	IDENTIFIER
Antibodies		
Anti-GAPDH	Abcam	AB_11129118
Anti-FXR1	Abcam	AB_11154960
Anti-SHP1	Abcam	AB_777912
Anti-SREBP1	Abcam	AB_777912
Anti-CHREBP	Abcam	AB_10562135
Anti-TGR5	Abcam	AB_2112165
Anti-Dio2 (D2)	Sigma-Aldrich	AB_10600804
Anti-UCP1 [EPR20381]	Abcam	AB_2722676
Anti-PGC 1 alpha	Abcam	AB_881987
Anti-mouse MUC2	Abcam	AB_10713220
Chemicals		
ampicillin	Sigma-Aldrich	Cat#171254-25GM
metronidazole	Sigma-Aldrich	Cat#M3761-25G
gentamicin	Sigma-Aldrich	Cat# E003632-10G
neomycin	Sigma-Aldrich	Cat# N6386-25G
vancomycin	Sigma-Aldrich	Cat# V2002-5G
CA	Sigma-Aldrich	Cat# C1129-25G
CDCA	Sigma-Aldrich	Cat# C9377-5G
LCA	Sigma-Aldrich	Cat# L6250-10G
DCA	Sigma-Aldrich	Cat# D6750-10G
TβMCA	Steraloids Inc	Cat# C1899-000
Critical Commercial Assays		
QIAamp DNA Stool Mini Kit	QIAGEN	Cat# 51504
Bile Acid Assay Kit	Sigma-Aldrich	Cat# MAK309
Mouse Leptin ELISA Kit	Sigma-Aldrich	Cat# RAB0334-1KT
TNF alpha Mouse ELISA Kit	Invitrogen	Cat# BMS607-3
Mouse IL-6 ELISA Kit	Sigma-Aldrich	Cat# RAB0308-1KT
Mouse LPS ELISA Kit	CUSABIO	Cat# CSB-E13066m
Software and Algorithms		
Prism 7.00	GraphPad	N/A
SPSS Statistics 20	IBM	N/A

Oligonucleotides

Gene	FORWARD PRIMER (5'-3')	REVERSE PRIMER (5'-3')	REF	SOURCE
Fungi ITS1	CTTGGTCATTTAGAGGAAGTAA	GCTGCGTTCTTCATCGATGC	[1]	Thermo Fisher
Universal	AGAGTTTGATCCTGGCTCAG	CTGCTGCCTCCCGTAGGAGT	[2]	Thermo Fisher
Bacteroidetes	GGARCATGTGGTTTAATTCGATGAT	AGCTGACGACAACCATGCAG	[2]	Thermo Fisher
Firmicutes	GGAGYATGTGGTTTAATTCGAAGCA	AGCTGACGACAACCATGCAC	[2]	Thermo Fisher
Akkermansia	CAGCACGTGAAGGTGGGGAC	CCTTGCGGTTGGCTTCAGAT	[3]	Thermo Fisher
Bilophila	CGGTATCGAAATCGTGAAGG	CAGAGGGTCAGGGTGTTGTT	[4]	Thermo Fisher
Desulfovibrio	CCGTAGATATCTGGAGGAACATCAG	ACATCTAGCATCCATCGTTTACAGC	[5]	Thermo Fisher
Bifidobacterium	GGGTGGTAATGCCGGATG	CCACCGTTACACCGGGAA	[6]	Thermo Fisher
Lactobacillus	AGCAGTAGGGAATCTTCCA	ATTYCACCGCTACACATG	[6]	Thermo Fisher
TJP1	TTTTTGACAGGGGGAGTGG	TGCTGCAGAGGTCAAAGTTCAAG	[7]	Thermo Fisher
Occludin	ATGTCCGGCCGATGCTCTC	TTTGGCTGCTCTTGGGTCTGTAT	[8]	Thermo Fisher
MUC2	TGTGGCCTGTGTGGGAACTTT	CATAGAGGGCCTGTCCTCAGG	[7]	Thermo Fisher
TLR4	GCAGAAAATGCCAGGATGATG	AACTACCTCTATGCAGGGATTCAAG	[7]	Thermo Fisher
TNFα	CGAGTGACAAGCCTGTAGCC	CATGCCGTTGGCCAGGA	[8]	Thermo Fisher
IL-6	TCCATCCAGTTGCCTTCTTG	TTCCACGATTTCCCAGAGAAC	[8]	Thermo Fisher
F4/80	CCCAGCTTATGCCACCTGCA	TCCAGGCCCTGGAACATTGG	[9]	Thermo Fisher
CEBPβ	GTTCTTGACGTTCTTCGGCCG	TGGACAAGCACAGCGACGAGT	[10]	Thermo Fisher
CEBPσ	AGTTTCTTGGGACATAGGAGCGCA	GTACCTTAGCTGCATCAACAGGAG	[11]	Thermo Fisher
CYP7A1	AGGACTTCACTCTACACC	GCAGTCGTTACATCATCC	[12]	Thermo Fisher
IBAT	GCCCCAAAAAGCAAAGATCA	GCTATGAGCACAATGAGGATGG	[13]	Thermo Fisher
FXRα1	CATCAGAGTACTTGAAGAAGATGTTGTCAGAGGACGG	CTCCTTCCGACATGGAGAAGTCATCGC	[14]	Thermo Fisher
FXRα2	GAAGGGGAGATGGTTTTGTTGTAAAGGCTCAAAG	TCTTGAAGACTGCATCTGTACCAGGGCCAT	[14]	Thermo Fisher
SHP	CCCTCCACAAACAATCCAGCCTTT	CATTAAGAGCCTGCCTGCGTTCAA	[14]	Thermo Fisher
SREBP-1c	CCAGCGGCTGCCTTCACACA	CCAGCCGAAAAGCGAGGCCA	[15]	Thermo Fisher
ChREBP	CGGGACATGTTTGATGACTATGTC	CATCCCATTGAAGGATTCAAATAAA	[16]	Thermo Fisher
PPARg1	GAGTGTGACGACAAGATTTG	GGTGGGCCAGAATGGCATCT	[17]	Thermo Fisher
PPARg2	TCTGGGAGATTCTCCTGTTGA	GGTGGGCCAGAATGGCATCT	[17]	Thermo Fisher
CD36	GGAACTGTGGGCTCATTGC	CATGAGAATGCCTCCAAACAC	[2]	Thermo Fisher
FAS	TGATGTGGAACACAGCAAG	GGCTGTGGTGACTCTTAGTGATAA	[2]	Thermo Fisher
GPAT	TCTGCTGCCATCTTTGTCCAC	TTGGTCTCTTTGAAAACCCCG	[2]	Thermo Fisher
FABP4	TTAAAAACACCGAGATTTCCTTCAA	GGGCCCCGCCATCTAG	[16]	Thermo Fisher
ATG-4b	TGGGTGTTATTGGAGGGAAG	CAGAAAAACCCCACAGCAAT	[15]	Thermo Fisher
ATG-5	TAGAATATATCAGACCACGACG	CTCCTCTTCTCTCCATCTTC	[15]	Thermo Fisher
ATG-7	TCCGTTGAAGTCCTCTGCTT	CCACTGAGGTTCACCATCCT	[15]	Thermo Fisher
CPT-1α	AGCACACCAGGCAGTAGCTT	AGGATGCCATTCTTGATTCG	[18]	Thermo Fisher
PPARα	GCGTACGGCAATGGCTTTAT	GAACGGCTTCCTCAGGTTCTT	[15]	Thermo Fisher
ACS	TATCATGCTTCACCTATGGC	CAAATAAGAGGAGCTCCAAC	[19]	Thermo Fisher
TGR5	GAGCGTCGCCCACCACTAGG	CGCTGATCACCCAGCCCCATG	[20]	Thermo Fisher
D2	CTTCCTCCTAGATGCCTACAAAC	GGCATAATTGTTACCTGATTCAGG	[21]	Thermo Fisher
UCP1	AGGCTTCCAGTACCATTAGGT	CTGAGTGAGGCAAAGCTGATTT	[22]	Thermo Fisher
PGC-1α	CCCCTTTGCCCTGACCTGCCTGAG	GAAGGACAGCTCTGATCACTGGCATTGG	[23]	Thermo Fisher
PRDM16	CAGCACGGTGAAGCCATTC	GCGTGCATCCGCTTGTG	[22]	Thermo Fisher

β-actin	GGATGCAGAAGGAGATCACTG	CGATCCACACGGAGTACTTG	24	Thermo Fisher

The bile acids standards including α-murocholic acid (αMCA), β-murocholic acid (βMCA), tauro-α-murocholic acid (TαMCA), tauro-β-murocholic acid (TβMCA), tauro-ursodesoxycholic acid (TUDCA), taurocholic acid (TCA), tauro-ursodeoxycholic acid (TDCA), glycocholic acid (GCA), glycodeoxycholic acid (GDCA), Cholic acid (CA), ursodeoxycholic acid (UDCA), hyodeoxycholic acid (HDCA), chenodeoxycholic acid (CDCA), deoxycholic acid (DCA), glycochenodeoxycholic acid (GCDCA), glycoursodeoxycholic acid (GUDCA), taurohyodeoxycholic acid (THDCA), taurolithocholic acid (TLCA), dehydrocholic acid (DHCA), lithocholic acid (LCA), [2,2,4,4-D4]-DCA (DCA-d4), [2,2,4,4-D4]-CA (CA-d4), [2,2,4,4-D4]-CDCA (CDCA-d4), [2,2,4,4-D4]-LCA (LCA-d4), [2,2,4,4-D4]-GCDCA (GCDCA-d4), [2,2,4,4-D4]-GCA (GCA-d4) were all purchased from Steraloids Inc (Newport, Rhode Island, USA).

CONTACT FOR REAGENT AND RESOURCE SHARING

Further information and requests for resources and reagents should be directed to and will be fulfilled by the Lead Contact, Zhan Jicheng (zhanjicheng@cau.edu.cn).

EXPERIMENTAL MODEL AND SUBJECT DETAILS

Animals

We performed three independent mouse studies to study the effect of BE on adiposity and its related metabolic syndromes based on high fat diet (HFD)- (studies 1 and 3) and genetically- (study 2)-induced obesity models. In study 1, male C57BL/6J mice purchased at 21 days of age (Vital River Laboratory Animal Technology. Co., Ltd., China) were randomly assigned to four groups (n = 9-12) after adapting for one week as follows: (1) a CHOW1 group fed a chow diet (3.85 kcal/g, 10% energy from fat) (D12450B, Research Diets, USA), (2) a HFD1 group fed a HFD (4.73 kcal/g, 60% energy from fat) (D12492, Research Diets), (3) a CBE group (5 gL^{-1} BE in drinking water) fed a chow diet, and (4) a BE1 group (0.5% (m/v) BE in drinking water) fed a HFD. In study 2, male C57BL/KsJ *db/db* mice purchased at 21 days of age (Model Animal Research Center of Nanjing University, Nanjing, China) were randomly assigned to two groups (n = 10) as follows: (1) a CHOW2 group fed a chow diet and (2) a BE2 group fed a chow diet with 5 gL^{-1} BE in drinking water. In study 3, male C57BL/6J mice purchased at 49 days of age (Vital River Laboratory Animal Technology. Co., Ltd.) were randomly assigned to five groups (n = 10-12) as follows: (1) a CHOW3 group fed a chow diet, (2) a HFD3 group fed a HFD, (3) a BE3 group (5 gL^{-1} BE in drinking water) fed a HFD, (4) an Abx group fed a HFD and (5) an ABE group (5 gL^{-1} BE in drinking water) fed a HFD. In study 3, all the mice were gavaged daily with 200 μL PBS containing (for the Abx and ABE groups) 0.5 mg ml^{-1} ampicillin, 0.5 mg ml^{-1} gentamicin, 0.5 mg ml^{-1} metronidazole, 0.5 mg ml^{-1} neomycin and 0.25 mg ml^{-1} vancomycin[25]

(Sigma-Aldrich, USA) or no antibiotics (for the CHOW3, HFD3 and BE3 groups).

Mice in all three studies were housed 3/cage in standard specific pathogen-free (SPF) conditions (12/12 h light/dark cycle, humidity of 50 ± 15%, temperature of 22 ± 2 ℃) and were allowed to adapt for one week before the experiments were started. The food used in these studies was sterilized using radiation (25.0 kGy). Food and water were provided *ad libitum*, and food intakes were recorded every week. Body weights were recorded weekly, the drinking water was changed every three days and fecal samples were collected at intervals. Mice eighteen weeks of age were fasted for 12 h in all mouse studies, plasma was dried in tubes following eyeball extirpation, and the mice were killed through breaking their necks immediately after taking the blood. After standing for 1 h, the blood was centrifuged at 3000 rpm for 10 min at 4℃ to obtain the blood plasma. The liver, inguinal white adipose tissue (iWAT), epididymal white adipose tissue (eWAT), brown adipose tissue (BAT), skeletal muscle, ileum and colon were obtained, weighed and placed into a 4% aqueous paraformaldehyde solution or liquid nitrogen immediately and then stored at -80℃ or room temperature for further analysis. The contents of the ileum, caecum, colon and rectum were collected and stored at -80℃ for GM analysis.

The guidelines of the National Institutes of Health regarding the care and use of laboratory animals were followed. This study was approved by the Animal Experiment Committee of the College of Food Science and Nutritional Engineering at China Agricultural University.

Cell Separation and Culture

The primary adipocytes were separated from the interscapular BAT of 5- to 6-week-old male mice, and the primary hepatocytes were separated from 8-week-old male mice using collagenase digestion and perfusion methods, respectively. Adipocyte differentiation was induced by treating confluent cells in DMEM (D-glucose, 25 mM) containing 10% fetal bovine serum (FBS), 0.5 mM isobutylmethylxanthine, 125 nM indomethacin, 1 mM dexamethasone, 850 nM insulin, 1 nM T3, 1 lM rosiglitazone, 100 U/ml penicillin, and 100 mg/ml streptomycin. After 2 days of induction, the cells were maintained in differentiation media (10% FBS, 850 nM insulin, 1 nM T3 and 1 lM rosiglitazone) in cell culture plates for the following experiment.[26] Hepatocytes were maintained in DMEM/F-12 (Gibco) with 10% FBS (Gibco), 1% ITS Liquid Media Supplement (Gibco), 40 ng/ml dexamethasone (Sigma), and 1% pen/strep (Gibco) in cell culture plates. All plates were incubated at 37℃ in 5% CO_2.

Adipocytes were treated with different concentrations (3 μM, 30 μM or 300 μM) of CDCA or LCA for 24 h, and then the cells were collected for mRNA expression and western blotting analysis. Hepatocytes were treated with or without CDCA (50 μM) and different concentrations (0, 100 μM or 300 μM) of TαMCA and TβMCA for 12 h for mRNA expression analysis and 24 h for western blotting analysis.

METHOD AND DETAILS

Extract and Analysis of the Phenolic Compounds in BE and Feces

The blueberries used in this study were highbush blueberries (*Vaccinium corymbosum*) grown in

the Daxing District, Beijing, China and harvested in 2016. The extraction and analysis of phenolic compounds from blueberries were performed as previously described with some modification.[27] Briefly, blueberry fruit or fresh feces was macerated and stirred with 95% ethanol (1:5, w (g)/v (ml)). The extract was then purified through an Amberlite XAD-7 column. The phenolic compounds were eluted with moderate absolute ethanol with 1% (v/v) formic acid. The eluent was concentrated under reduced pressure at 35°C and freeze-dried.

The total polyphenol content in the BE was determined with a modified Folin-Ciocalteu method, and the total anthocyanin content of the BE was directly determined using a pH differential method as previously described.[27] The results are presented as mg gallic acid or cyanidin-3-O-glucoside equivalent/100 mg of BE, respectively.

The concentrations of phenolic compounds in the BE and anthocyanins in the feces were determined with a UPLC (Waters, Milford, MA, USA) equipped with a QqQ-MS and diode array detector (DAD) as described with some modifications.[28] Chromatographic separations were performed on an Acquity UPLC HSS T3 (Waters) column (2.1× 100 mm, 1.7 μm). The injection volume was 2 μL, and a 0.4 mL/min flow rate was used. The mobile phase consisted of 2 phases: (A) and (B). Mobile phase (A) was 5% (v/v) formic acid in water, and mobile phase (B) was 5% (v/v) formic acid in acetonitrile. BE and FE were dissolved in mobile phase (A) and filtered through a 0.22 μm membrane filter. The elution conditions were as follows: 0~0.5 min, 99% A; 0.5~16 min, 99~65% A; 16~18 min, 65~0% A; 18~21 min, 0% A; 21~23 min, 0~99% A; 23~23.5 min, 99% A. The column temperature was 40°C, and the detection wavelength was 520 nm (for the determination of anthocyanins).

Determination of the Composition and Concentration of Bile Acids in the Plasma through LC-MS

The plasma composition and concentration of twenty common bile acids were determined through UPLC/electrospray ionization mass spectrometry (UPLC/ESI-MS) as described with some modification.[29] Briefly, one milliliter of precooled ethanol was added to a 50 μL plasma sample. Following vortex and centrifugation, the supernatant was then filtered with a 0.22 μm filter before analysis with LC-MS.

Liquid chromatography (LC) separation was performed using a Waters Acquity UPLC system with a BEH C18 column (1.7 μm, 100 mm, 2.1 mm; Waters) and maintained at 40°C. The sample injection volume was 1 μL. Solvent A was water containing 0.005% (v/v) formic acid. Solvent B was acetonitrile containing 0.005% formic acid, and the flow rate was 0.4 mL/min. The gradient program was as follows: 0 ~ 2 min, 77% ~ 67% A; 2 ~ 6 min, 67% ~ 66% A; 6 ~ 11 min, 66% ~ 30% A. MS analysis was performed using a Quattro Premier XE quadrupole tandem MS (Waters) equipped with an ESI probe in negative-ion mode. A capillary voltage of -3,200 V, a source temperature of 120°C, and a desolvation temperature of 400°C were used. The concentrations of individual BAs were calculated from the peak area in the chromatogram detected with selected ion recording relative to that of the internal standard, nordeoxycholic acid.

Quantitative Real-time PCR (qPCR) Analysis

Total RNA was extracted using TRIzol™ reagent (Invitrogen) according to the manufacturer's instructions. Reverse transcription of the total RNA (2.5 μg) was performed with a high-capacity cDNA reverse transcription kit (Promega Biotech Co., Ltd). qPCR was run in triplicate for each sample and analyzed in a LightCycler 480 real-time PCR system (Roche). Data were normalized to the internal control *β-actin* and analyzed using the △△CT method.[30] The expression of genes related to lipid metabolism (in the WAT, BAT and liver), inflammation (in the WAT and liver), permeability (in the ileum and colon), and thermogenesis (in the BAT), as well as the bacterial load, were determined through qPCR (the related genes and primers used are shown in Table S1).

Quantification of the bacterial load through qPCR was conducted as previously described.[30] Briefly, the total bacterial DNA was isolated from the samples with a QIAamp DNA Stool Mini Kit (Qiagen). The DNA was then subjected to qPCR using a QuantiFast SYBR Green PCR kit (Bio-Rad) with universal 16S rRNA primers (Table 1).[2] The results are expressed as bacterial number per g of sample using a standard curve made using *Bifidobacterium longum*.

Metabolic Rate and Physical Activity

Oxygen consumption and physical activity were determined in 16-week-old mice before a GTT. Oxygen consumption was measured using TSE lab master systems as previously described.[22] All mice were acclimatized for 24 h prior to the measurements, and then VO_2 and VCO_2 were measured over the course of 24 h. The mice were maintained at 25°C under a 12 h light/dark cycle with free access to food and water. Their physical activity was measured by the optical beam technique (Opto-M3; Columbus Instruments, Columbus, OH, USA) over 24 h and calculated as 24 h average activity.

Positron Emission Tomography-Computed Tomography and Transmission Electron Microscopy

At the end of the experiment, the mice fasted overnight. After exposure to a cold environment (4°C) for 30 min, the mice were lightly anesthetized with isoflurane and injected with 18F-FDG (500 mCi) via the tail vein. Sixty minutes after radiotracer injection, the mice were subjected to PET/CT imaging with the Siemens Inveon Dedicated PET (dPET) system and an Inveon Multimodality System (CT/SPECT) (Siemens Preclinical Solutions, Knoxville, TN, USA) at the Institute of Laboratory Animal Sciences, Chinese Academy of Medical Sciences. Inveon Acquisition Workplace software was used for the scanning process. The positron emission tomography-computed tomography (PET-CT) instrument parameters were as previously described, and data analysis was performed as previously described.[31]

BAT sections were fixed with 2% (v/v) glutaraldehyde in 0.1 M phosphate buffer (pH 7.4) for 12 h at 4°C. The sections were then postfixed with 1% osmium tetroxide, dehydrated in ascending concentrations of ethanol, and embedded in fresh epoxy resin 618. Ultrathin sections (60–80 nm) were cut and stained with lead citrate before being examined on a Hitachi H-7500 transmission electron microscope.

MRI

MRI experiments were performed on 15-week-old mice. MRI measurements were performed on a 7.0 T Varian MRI instrument (Varian Medical Systems, Palo Alto, CA, USA) using a 40 mm volume and receiver coil at the Institute of Laboratory Animal Sciences, Chinese Academy of Medical Sciences. Prior to the experiments, the mice were initially anesthetized with 2% isoflurane in a dedicated chamber. During the course of MRI, anesthesia levels were reduced to 1.5–1% in a combination of medical air and medical oxygen. The mice were positioned in the prone position, and respiratory-gated image acquisition was performed. MRI images of the mice were analyzed by Argus software.

Glucose and Insulin Tolerance Tests (GTT and ITT)

A GTT was performed on 16-week-old mice after a 16 h fast. Glucose concentrations were measured in blood collected by venous bleeding from the tail vein before and 15 min, 30 min, 45 min, 60 min, 90 min, and 120 min after an intraperitoneal injection of 1.5 g/kg • body weight glucose using a Roche Diabetes Care glucometer (Roche, Germany).

An ITT was conducted on 17-week-old mice after a 6 h fast. Glucose concentrations were measured in blood collected by venous bleeding before and 15 min, 30 min, 45 min, and 60 min after the injection of insulin (Novolin, 30 R, 1.0 U/kg • body weight).

Plasma Parameters

The plasma biochemical parameters, including alanine transaminase (ALT), glucose, cholesterol, triglyceride (TG), high-density lipoprotein cholesterol (HDL-C), low-density lipoprotein cholesterol (LDL-C), and lactate dehydrogenase (LDH) levels, were determined by a 3100 Clinical Analyzer (Hitachi High-Technologies Corporation, Japan). The level of the plasma inflammation factor LPS was determined with an enzyme-linked immunosorbent assay (ELISA) kit (Thermo Fisher, USA) according to the operating instructions.

Histology and Oil Red O Staining

Tissues fixed in 4% paraformaldehyde were cut into 5 μm sections after being embedded in paraffin. Multiple sections were prepared and stained with hematoxylin and eosin (H&E) for general morphological observation.

Oil red O staining was performed as described by Ross et al.[32] Briefly, liver slices were washed with phosphate-buffered saline, fixed in 3.7% formaldehyde for 2 min, washed with H_2O, incubated with oil red O solution for 1 h at room temperature, and then washed with H_2O.

Immunohistochemistry and Immunofluorescence

Tissue sections for immunohistochemical testing were prepared on poly-L-lysine-pretreated

coverslips. Immunohistochemical staining was performed according to a standard protocol using antibodies against UCP1, TGR5, FXR1, SHP1 and SREBP-1c at a 1:500 dilution. The samples were incubated overnight in a humidified chamber at 4°C. Secondary antibodies for immunohistochemical staining were purchased from Invitrogen. All images were acquired on an Olympus BX51 system and processed using ImageJ software, version 1.8.0.
Immunostaining for mucin 2 was conducted using MUC2 primary antibody at a 1:1000 dilution. The samples were incubated overnight at 4°C. Secondary antibodies for immunofluorescence staining were diluted to 1:1500 and applied to the section for 2 h. Observations and analyses were performed with a Zeiss LSM 700 confocal microscope.

Western Blotting

Homogenized tissues were lysed in RIPA buffer containing protease and phosphatase inhibitors. The protein lysates were separated by SDS-PAGE. After electrophoresis, the proteins were transferred to a polyvinylidene difluoride membrane (Millipore), incubated with blocking buffer (5% fat-free milk) for 1 h at room temperature, and then blotted with the following antibodies overnight: anti-UCP1, anti-TGR5, anti-D2, anti-PGC-1α, anti-FXR1, anti-SHP1, anti-SREBP1 and anti-GAPDH. The membrane was incubated with HRP-conjugated secondary antibodies for 1 h at room temperature. The intensity values of the bands were quantified using ImageJ software.

Bomb Calorimetry

Fecal samples were collected from individual mice during the last week of the experiment and used for bomb calorimetry analysis. For bomb calorimetry analysis, the samples were weighed and oven-dried at 608°C for 48 h. The energy content of the feces was assessed with a Parr 6100 calorimeter using a 1109 semimicro bomb (Parr Instrument Co., Moline, Illinois, USA). The calorimeter energy equivalent factor was determined using benzoic acid standards, and each sample (100 mg) was analyzed in triplicate.

GM Analysis

The GM of the mice was analyzed as previously described.[30] Total genomic DNA was extracted from pooled samples using the CTAB/SDS method. The DNA concentration and purity were monitored on 1% agarose gels, and the DNA was diluted to 1 ng/μl in sterile water. 16S rRNA genes were amplified using a specific primer with a barcode. PCR was conducted in 30 μL reactions with 15 μL Phusion® High-Fidelity PCR Master Mix (New England Biolabs, USA), 0.2 μM forward and reverse primers, and approximately 10 ng template DNA. Thermal cycling consisted of an initial denaturation at 98 ℃ for 1 min, followed by 30 cycles of denaturation at 98 ℃ for 10 s, annealing at 50 ℃ for 30 s, and elongation at 72 ℃ for 30 s and, finally, 72 ℃ for 5 min. The PCR products were mixed in equal parts. The mixture was purified using a GeneJET Gel Extraction Kit (Thermo Scientific, USA). Sequencing libraries were generated using a TruSeq® DNA PCR-Free Sample Preparation Kit, following the manufacturer’s recommendations. Index codes were added. The library quality was assessed on a Qubit@ 2.0 Fluorometer (Thermo

Scientific) and an Agilent Bioanalyzer 2100 system. Finally, the library was sequenced on an Illumina HiSeq 2500, and 250 bp paired-end reads were generated.

Paired-end reads from the original DNA fragments were merged by using FLASH,[33] a high-speed and accurate analysis tool designed to merge paired-end reads when overlaps exist between read 1 and read 2. Paired-end reads were assigned to each sample according to their unique barcodes. The sequences were analyzed using the QIIME[34] (Quantitative Insights Into Microbial Ecology) software package. In-house Perl scripts were used to analyze alpha- (within samples) and beta- (among samples) diversity. First, the reads were filtered by QIIME quality filters. Then, pick_de_novo_otus.py was used to pick operational taxonomic units (OTUs) by creating an OTU table. Sequences with ≥ 97% similarity were assigned to the same OTUs. We picked a representative sequence for each OTU and used RDP classifier[35] to annotate taxonomic information for each representative sequence.

Statistical Analysis

All data reported in this paper are expressed as the means ± SEs. The data were evaluated by one-way ANOVA followed by Duncan's significant difference test. All statistics were analyzed by SPSS software, and all analyses were performed with GraphPad Prism 7.

REFERENCE

1. Jiang, T. T.; Shao, T. Y.; Ang, W. X. G.; Kinder, J. M.; Turner, L. H.; Pham, G.; Whitt, J.; Alenghat, T.; Way, S. S., Commensal Fungi Recapitulate the Protective Benefits of Intestinal Bacteria. *Cell host & microbe* **2017,** *22* (6), 809-816 e4.
2. Cho, I.; Yamanishi, S.; Cox, L.; Methe, B. A.; Zavadil, J.; Li, K.; Gao, Z.; Mahana, D.; Raju, K.; Teitler, I.; Li, H.; Alekseyenko, A. V.; Blaser, M. J., Antibiotics in early life alter the murine colonic microbiome and adiposity. *Nature* **2012,** *488* (7413), 621-626.
3. Zhang, Z.; Wu, X.; Cao, S.; Cromie, M.; Shen, Y.; Feng, Y.; Yang, H.; Li, L., Chlorogenic acid ameliorates experimental colitis by promoting growth of Akkermansia in mice. *Nutrients* **2017,** *9* (7), 677.
4. Jena, P. K.; Sheng, L.; Nagar, N.; Wu, C.; Barile, D.; Mills, D. A.; Wan, Y.-J. Y., The effect of synbiotics Bifidobacterium infantis and milk oligosaccharides on shaping gut microbiota community structure and NASH treatment. *Data in brief* **2018,** *19*, 1025-1029.
5. Christophersen, C.; Morrison, M.; Conlon, M., Overestimation of the abundance of sulfate-reducing bacteria in human feces by quantitative PCR targeting the Desulfovibrio 16S rRNA gene. *Appl. Environ. Microbiol.* **2011,** *77* (10), 3544-3546.
6. Ritchie, L. E.; Burke, K. F.; Garcia-Mazcorro, J. F.; Steiner, J. M.; Suchodolski, J. S., Characterization of fecal microbiota in cats using universal 16S rRNA gene and group-specific primers for Lactobacillus and Bifidobacterium spp. *Veterinary microbiology* **2010,** *144* (1-2), 140-146.
7. Tilg, H.; Cani, P. D.; Mayer, E. A., Gut microbiome and liver diseases. *Gut* **2016,** *65* (12), 2035-2044.
8. Zou, J.; Chassaing, B.; Singh, V.; Pellizzon, M.; Ricci, M.; Fythe, M. D.; Kumar, M. V.; Gewirtz, A. T., Fiber-mediated nourishment of gut microbiota protects against diet-induced obesity by restoring

IL-22-mediated colonic health. *Cell host & microbe* **2018,** *23* (1), 41-53. e4.

9. Moriguchi, T.; Yu, L.; Otsuki, A.; Ainoya, K.; Lim, K.-C.; Yamamoto, M.; Engel, J. D., Gata3 hypomorphic mutant mice rescued with a yeast artificial chromosome transgene suffer a glomerular mesangial cell defect. *Molecular and cellular biology* **2016,** *36* (17), 2272-2281.

10. Wen, C.-L.; Teng, C.-L.; Chiang, C.-H.; Chang, C.-C.; Hwang, W.-L.; Kuo, C.-L.; Hsu, S.-L., Methanol extract of Antrodia cinnamomea mycelia induces phenotypic and functional differentiation of HL60 into monocyte-like cells via an ERK/CEBP-β signaling pathway. *Phytomedicine* **2012,** *19* (5), 424-435.

11. Hyldahl, R. D.; Xin, L.; Hubal, M. J.; Moeckel-Cole, S.; Chipkin, S.; Clarkson, P. M., Activation of nuclear factor-κB following muscle eccentric contractions in humans is localized primarily to skeletal muscle-residing pericytes. *The FASEB Journal* **2011,** *25* (9), 2956-2966.

12. Zang, R.; Li, D.; Tang, I.-C.; Wang, J.; Yang, S.-T., Cell-based assays in high-throughput screening for drug discovery. *International Journal of Biotechnology for Wellness Industries* **2012,** *1* (1), 31-51.

13. Ho, R. H.; Leake, B. F.; Urquhart, B. L.; Gregor, J. C.; Dawson, P. A.; Kim, R. B., Functional characterization of genetic variants in the apical sodium‐dependent bile acid transporter (ASBT; SLC10A2). *Journal of gastroenterology and hepatology* **2011,** *26* (12), 1740-1748.

14. Howarth, D. L.; Law, S. H.; Law, J. M.; Mondon, J.; Kullman, S. W.; Hinton, D. E., Exposure to the synthetic FXR agonist GW4064 causes alterations in gene expression and sublethal hepatotoxicity in eleutheroembryo medaka (Oryzias latipes). *Toxicology and applied pharmacology* **2010,** *243* (1), 111-121.

15. Martinez-Lopez, N.; Tarabra, E.; Toledo, M.; Garcia-Macia, M.; Sahu, S.; Coletto, L.; Batista-Gonzalez, A.; Barzilai, N.; Pessin, J. E.; Schwartz, G. J., System-wide benefits of intermeal fasting by autophagy. *Cell metabolism* **2017,** *26* (6), 856-871. e5.

16. Bäckhed, F.; Ding, H.; Wang, T.; Hooper, L. V.; Koh, G. Y.; Nagy, A.; Semenkovich, C. F.; Gordon, J. I., The gut microbiota as an environmental factor that regulates fat storage. *Proceedings of the National Academy of Sciences* **2004,** *101* (44), 15718-15723.

17. Zhang, Y.-L.; Hernandez-Ono, A.; Siri, P.; Weisberg, S.; Conlon, D.; Graham, M. J.; Crooke, R. M.; Huang, L.-S.; Ginsberg, H. N., Aberrant hepatic expression of PPARγ2 stimulates hepatic lipogenesis in a mouse model of obesity, insulin resistance, dyslipidemia, and hepatic steatosis. *Journal of Biological Chemistry* **2006,** *281* (49), 37603-37615.

18. Bäckhed, F.; Manchester, J. K.; Semenkovich, C. F.; Gordon, J. I., Mechanisms underlying the resistance to diet-induced obesity in germ-free mice. *Proceedings of the National Academy of Sciences* **2007,** *104* (3), 979-984.

19. Tsuda, T.; Horio, F.; Uchida, K.; Aoki, H.; Osawa, T., Dietary cyanidin 3-O-β-D-glucoside-rich purple corn color prevents obesity and ameliorates hyperglycemia in mice. *The Journal of nutrition* **2003,** *133* (7), 2125-2130.

20. Kumar, D. P.; Rajagopal, S.; Mahavadi, S.; Mirshahi, F.; Grider, J. R.; Murthy, K. S.; Sanyal, A. J., Activation of transmembrane bile acid receptor TGR5 stimulates insulin secretion in pancreatic β cells. *Biochemical and biophysical research communications* **2012,** *427* (3), 600-605.

21. Marsili, A.; Ramadan, W.; Harney, J. W.; Mulcahey, M.; Castroneves, L. A.; Goemann, I. M.; Wajner, S. M.; Huang, S. A.; Zavacki, A. M.; Maia, A. L., Type 2 iodothyronine deiodinase levels are higher in slow-twitch than fast-twitch mouse skeletal muscle and are increased in hypothyroidism. *Endocrinology* **2010,** *151* (12), 5952-5960.

22. You, Y. L.; Han, X.; Guo, J. L.; Guo, Y.; Yin, M. W.; Liu, G. J.; Huang, W. D.; Zhan, J. C., Cyanidin-3-glucoside attenuates high-fat and high-fructose diet-induced obesity by promoting the

thermogenic capacity of brown adipose tissue. *Journal Of Functional Foods* **2018,** *41*, 62-71.

23. Albertoni, G.; Schor, N., Resveratrol plays important role in protective mechanisms in renal disease-mini-review. *Brazilian Journal of Nephrology* **2015,** *37* (1), 106-114.

24. Sevelda, F.; Mayr, L.; Kubista, B.; Lötsch, D.; van Schoonhoven, S.; Windhager, R.; Pirker, C.; Micksche, M.; Berger, W., EGFR is not a major driver for osteosarcoma cell growth in vitro but contributes to starvation and chemotherapy resistance. *Journal of Experimental & Clinical Cancer Research* **2015,** *34* (1), 134.

25. Elahi, S.; Ertelt, J. M.; Kinder, J. M.; Jiang, T. T.; Zhang, X.; Xin, L.; Chaturvedi, V.; Strong, B. S.; Qualls, J. E.; Steinbrecher, K. A.; Kalfa, T. A.; Shaaban, A. F.; Way, S. S., Immunosuppressive CD71+ erythroid cells compromise neonatal host defence against infection. *Nature* **2013,** *504* (7478), 158-62.

26. Li, Y.; Fromme, T.; Schweizer, S.; Schottl, T.; Klingenspor, M., Taking control over intracellular fatty acid levels is essential for the analysis of thermogenic function in cultured primary brown and brite/beige adipocytes. *EMBO Rep* **2014,** *15* (10), 1069-76.

27. You, Y.; Yuan, X.; Lee, H. J.; Huang, W.; Jin, W.; Zhan, J., Mulberry and mulberry wine extract increase the number of mitochondria during brown adipogenesis. *Food & function* **2014,** *6* (2), 401.

28. Goncalves, J.; Mendes, B.; Silva, C. L.; Camara, J. S., Development of a novel microextraction by packed sorbent-based approach followed by ultrahigh pressure liquid chromatography as a powerful technique for quantification phenolic constituents of biological interest in wines. *J Chromatogr A* **2012,** *1229*, 13-23.

29. Hagio, M.; Matsumoto, M.; Fukushima, M.; Hara, H.; Ishizuka, S., Improved analysis of bile acids in tissues and intestinal contents of rats using LC/ESI-MS. *J Lipid Res* **2009,** *50* (1), 173-80.

30. Guo, J. L.; Han, X.; Zhan, J. C.; You, Y. L.; Huang, W. D., Vanillin Alleviates High Fat Diet-Induced Obesity and Improves the Gut Microbiota Composition. *Frontiers In Microbiology* **2018,** *9:2733.*

31. Yuan, X.; Wei, G.; You, Y.; Huang, Y.; Lee, H. J.; Dong, M.; Lin, J.; Hu, T.; Zhang, H.; Zhang, C.; Zhou, H.; Ye, R.; Qi, X.; Zhai, B.; Huang, W.; Liu, S.; Xie, W.; Liu, Q.; Liu, X.; Cui, C.; Li, D.; Zhan, J.; Cheng, J.; Yuan, Z.; Jin, W., Rutin ameliorates obesity through brown fat activation. *FASEB J* **2017,** *31* (1), 333-345.

32. Ross, S. E.; Erickson, R. L.; Hemati, N.; Macdougald, O. A., Glycogen Synthase Kinase 3 Is an Insulin-Regulated C/EBPα Kinase. *Molecular & Cellular Biology* **1999,** *19* (12), 8433.

33. Magoč, T.; Salzberg, S. L., FLASH: fast length adjustment of short reads to improve genome assemblies. *Bioinformatics* **2011,** *27* (21), 2957-2963.

34. Caporaso, J. G.; Kuczynski, J.; Stombaugh, J.; Bittinger, K.; Bushman, F. D.; Costello, E. K.; Fierer, N.; Pena, A. G.; Goodrich, J. K.; Gordon, J. I., QIIME allows analysis of high-throughput community sequencing data. *Nature methods* **2010,** *7* (5), 335.

35. Wang, Q.; Garrity, G. M.; Tiedje, J. M.; Cole, J. R., Naïve Bayesian Classifier for Rapid Assignment of rRNA Sequences into the New Bacterial Taxonomy. *Applied & Environmental Microbiology* **2007,** *73* (16), 5261.